Analysis of Wave Characteristics in the Coastal Waters of Bangladesh Using Buoy and Model Data

N.C.V. Ross

Bachelor Thesis

20 June 2024

Colophon

Title	Analysis of Wave Characteristics in the Coastal Waters of Bangladesh Using Buoy and Model Data
Version	Draft
Research period	April to June 2024
Date of publication	20-06-2024
Picture on front page	Buoy at the sea of Iran retrieved from *Cargo & Sea Management* (n.d.)

Author	N.C.V. (Naomi) Ross
Student number	S2681846
E-mail	n.c.v.ross@student.utwente.nl

Internal supervisor	Dr.Ir. P.C. (Pieter) Roos
Second assessor	PhD. M. (Monica) Pena Acosta

Involved company	WaterProof Marine Consultancy & Services BV.
External supervisors	PhD. N. (Nathanaël) Geleynse PhD. R. (Rinse) de Swart

Abstract

Understanding wave patterns in the Bay of Bengal is crucial due to the increasing intensity of tropical storms caused by climate change and rising sea levels, which pose significant risks to the coastal areas of Bangladesh. Additionally, the channel at the sea near the Port of Payra has been deepened to boost Bangladesh' international trades. Therefor, an analysis of the significant wave height and wave directions along the coast and offshore of Bangladesh can provide the impact of cyclones and changes of wave characteristics caused by the channel.

The first part of this research focuses on investigating the significant wave heights and wave directions using three datasets: buoy measurements, the WaveWatch III (WW3) model, and the SWAN model. The buoy data provides real-time observations of wave conditions, while the WW3 and SWAN models offer numerical simulations based on wind data. This analysis provides the significant wave heights of different locations and the corresponding wave directions, showing the impact of seasonal variations and cyclonic storm events on the wave patterns.

In the second part, the three datasets are compared to evaluate their accuracy and reliability. The analysis concluded that the significant wave height of the buoy measurements decreases as the waves propagate towards the coast, while the wave direction remains aligned with the channel. The WW3 model provides wave data for a point further offshore than KP60, showing significant wave height values slightly higher than KP60. The SWAN model also shows slightly higher values at the WW3 point. The wave directions align with the buoy measurement data, corresponding to the channel direction and refract when the channel direction slightly shifts.

Contents

1 Introduction

Today, the world is facing climate change, characterised by rising temperatures, higher sea levels and more frequent and severe storms. In the Netherlands, even a slight sea level increase has significant impact, as a large part of the country lies below sea level. The Netherlands is not the only country facing these environmental challenges. Bangladesh, located on the northern coast of the Bay of Bengal in Asia as seen in Figure 1.1, is also facing similar issues. Approximately a quarter of Bangladesh's landmass is situated less than 2 meters above sea level. Additionally, Bangladesh is ranked sixth on the 2018 global climate risk index indicating to what extent countries have been affected by the impacts of weather-related loss events (storms, floods, heat waves etc.) (NRDC, 2018). The rising sea levels pose a threat to the low-lying highly populated coastal areas and cause an increased risk of saltwater intrusion that jeopardize the agriculture and the drinking water supplies (NRDC, 2018).

Figure 1.1: The locations of Bangladesh located in the Bay of Bengal in relation to the world (WorldAtlas, n.d.)

The Bay of Bengal experiences three to four tropical cyclones yearly, with their intensity rising due to changing environmental factors (Balaguru et al., 2014). This trend may continue in the future, causing widespread flooding and devastation along the coast. (NRDC, 2018).

Moreover, countries worldwide are striving to compete in the global market. This goal is also shared by Bangladesh, which aims to establish the Port of Payra on its coast to enhance import and export opportunities, positioning Bangladesh as a key player in the nation's international trade. In 2016 a channel has been created starting 57 km off the coast of Bangladesh towards the Port of Payra. Figure 1.2 shows the location of the port. The deepening of the channel began in 2022, and since then, it has been maintained at the same depth through regular dredging (de Nul, n.d.).

Analysing wave characteristics offshore and along the coast of Bangladesh is important for accessing the impact of cyclones and changes of wave characteristics caused by the channel. Additionally, the wave characteristics vary based on the seasons. Bangladesh has three distinct

seasons: a hot and humid summer from March to June; a cool and rainy monsoon season from June to October; and a cool and dry winter from October to March. This thesis gives the wave characteristic variations in the Bay of Bengal along the channel, spanning from offshore to nearshore regions throughout the year.

Figure 1.2: The location of the Port of Payra in relation with Bangladesh (WorldAtlas, n.d.).

In this paper, the wave characteristics will be derived from buoy measurements and from the Wave Watch III (WW3) and SWAN models. Both models are based on wind data and will be explained in Section 2.3.

1.1 Context

1.1.1 Research motivation

As already mentioned in the introduction, due to climate change more tropical storms are formed and because of the rising sea level the coast of Bangladesh is exposed to higher waves causing the salt water to infiltrate in the coast land of Bangladesh. The cyclonic storm Mocha which caused big floods and erosion at the coast in 2023 is an example of why it is important to understand the wave patterns in the Bay of Bengal towards the coast of Bangladesh (WMO, 2023).

Identifying the present-day wave characteristics at the Bay of Bengal and how the waves change from offshore to nearshore of Bangladesh is necessary to predict wave patterns in the future. In addition, the sediment transport paths near the coast can be determined and the water heights and wave breaks during storm surges can be predicted.

The engineering consultancy firm WaterProof (Lelystad, The Netherlands) is commissioned by Jan de Nul (Aalst, Belgium) to investigate the sediment transport paths in the channel that

connects the Port of Payra with the Bay of Bengal. The sediment transport paths can be identified by knowing the wave characteristics in the offshore and nearshore of this channel.

1.1.2 Problem statement

Since, the channel has been deepened in 2021 and 2022, little is known about the effects the channel has on the waves near the channel. This thesis aims to investigate the change in wave characteristics from offshore to nearshore along the channel. Understanding these wave characteristics near the channel is crucial for the sediment change in the seabed around and in the channel.

1.2 Literature review

This section reviews two studies about the waves near the coast of Bangladesh. Additionally, a study about how waves act near a channel.

1.2.1 Wave patterns at the Bay of Bengal with the Delft3D model

Matin et al. (2020) have analysed the significant wave height, the mean direction and the typical depth-average current velocity have been analysed in the wet and dry season. Additionally, the significant wave height at eight locations near the coast of Bangladesh. These wave characteristics are estimated based on a coupled Delft3D and SWAN model. This modelling system is based on a 2D mathematical model containing the continuity equation and momentum equations. The model incorporates wind data from European Centre for Medium-Range Weather Forecasts (ECMWF), an estimated Manning's roughness coefficient and measured boundary wave heights.

Figure 1.3 shows the significant wave height in the Bay of Bengal for the highest waves in the wet (monsoon) season and average waves in the dry season. Both figures reveal that the prominent shoaling effect was observed as the wave approaches the continental shelf from the deep waters of the bay. Figure 1.4 shows the mean wave direction for the wet and dry season. On May 21st, the wave direction is primarily from the South-Southeast, while on December 8th, it is mainly from North-Northwest.

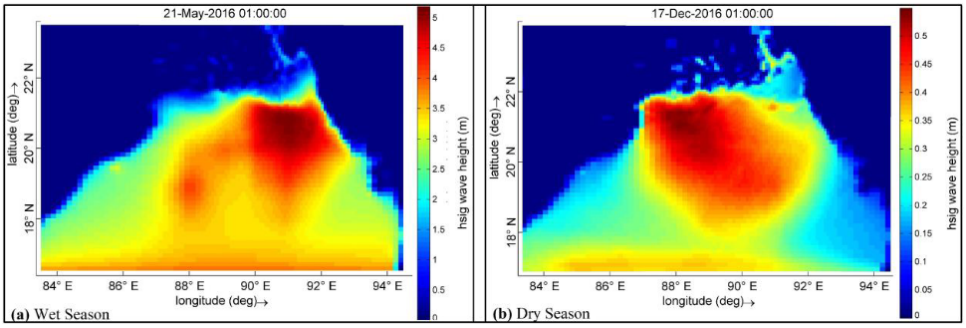

Figure 1.3: Typical significant wave height in the Bay of Bengal during (a) the wet season and (b) the dry season (Matin et al., 2020)

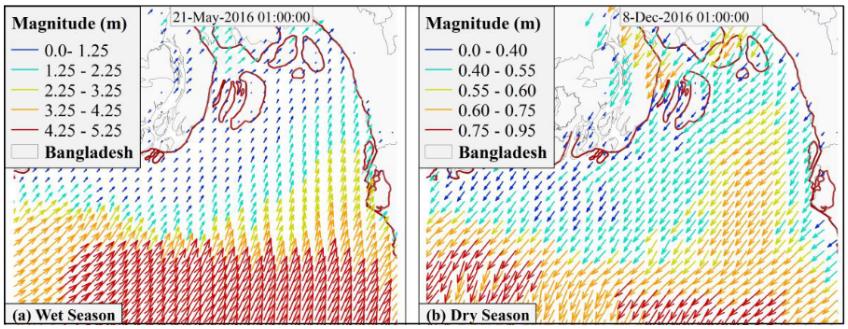

Figure 1.4: Typical mean wave direction near the Bangladesh coast in (a) wet season (b) dry season (Matin et al., 2020)

Matin et al. (2020) further provides simulated significant wave heights from eight locations in 2016 which are shown in Figure 1.5. Kuakata is the closest location to the cahnnel and the simulated significant wave height is shown in Figure 1.6.The significant wave height during the wet season is the highest, followed by a decrease in the dray season, except for sudden short peaks.

The model used in this paper focuses on waves at a large scale. It can therefore not capture the influence of the channel. Additionally, the Manning's roughness factor was calibrated using data from 2016 only, thus the factor may not be accurate for other years. This thesis will analyse wave characteristics near the channel over multiple years to determine if the channel has an affect on these wave characteristics. Moreover, this thesis will ensure that observed wave heights are consistent across different years.

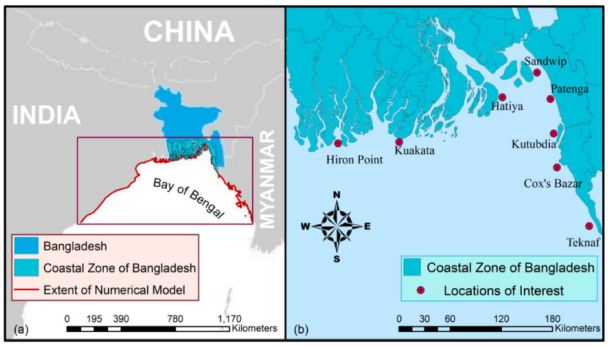

Figure 1.5: The location of Kuakata visualised at the coast of Bangladesh

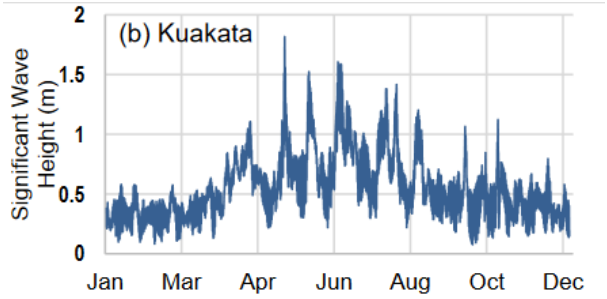

Figure 1.6: Simulated significant wave height at Kuakata of the year 2016

1.2.2 Wave characteristics in the Southeastern Bengal Bay based on different data sources

In a second study, Xu et al. (2021), the wave direction and wave height are compared based on different datasets: Ocean Weather wave data (OWI) and ECMWF data. The OWI data includes all data of wind fields 10 meter above the global sea level released by United States, while the ECMWF is an intergovernmental organization that provides global weather data and forecasts. This analysis compares the wave direction and wave height resulted from OWI data and ECMWF data. Additionally, these two datasets are compared with the SWAN model.

Figure A.1 shows the total wave rose derived from ECMWF data. The seasonal wave roses for both ECMWF and IWO data are displayed in Appendix A. These figures indicate that the significant wave heights of the ECMWF data are higher and that the wave directions differ slightly between the two models. Additionally, the paper gives for both datasets the relation between swell and wind waves, seen in Table 1. The Table shows that for the wave direction of SW, the swell waves are dominant for both data sets and differ slightly. For the NW direction, there are large differences in the ratio of wind and swell waves and therefore the SWAN model is used as an additional dataset. The results of the SWAN model in the NW direction for the wind and swell waves are 76.1% and 23.9% respectively.

Table 1: The relation between swell and wind wave for wave directions of the datasets ECMWF and OWI. For the NW direction the SWAN model also provides the relation.

	ECMWF data	OWI data	SWAN model
SW wind waves (%)	13.4	24.5	-
SW swell waves (%)	86.6	75.4	-
NW wind waves (%)	24.5	62.6	76.1
NW swell waves (%)	75.4	37.4	23.9
NW wave period (s)	7.26	5.6	5.0

Xu et al. (2021) concludes that in the SW direction the swell waves are dominant as the length of the wind zones are nearly 900 km. In contrast, in the NW direction the wind waves are dominant as the length from the southeast coast to the NW coast are relatively short. The paper's scope is limited to the southeast coast of Bangladesh, offering only a single wave rose at one location. This paper also considers only data for one year. The aim of this thesis is to investigate wave characteristics at multiple locations with the focus on the wave transition from offshore to nearshore along the channel.

1.2.3 Modelling refraction of waves over tidal channels

A third study by van der Reijden (2020) investigates the wave heights near a tidal channel in the Eastern Wadden Sea under varying wave directions using the Ray-tracing model REFRAC and the spectral model SWAN. This study gives insights into the wave heights near and within the channel of the two models for different angels relative to the channel. The relative results from van der Reijden (2020) are for a wave direction of 320 degrees, when the wave direction is almost parallel to the channel.

In figure 1.7 the wave heights of the direction of 320 degrees for the periods of 5, 10 and 15 seconds can be seen. A period of 5 seconds corresponds to wind waves, while a period of 15 seconds corresponds to swell waves. A period of 10 seconds is considered to be on the boundary between wind and swell waves. The wave heights for periods of 10 to 15 seconds show somewhat similar wave heights, while the wave heights for the period of 5 seconds are significantly lower.

The figure also shows that the wave heights in the channel are lower, while on both sides of the channel the wave heights are higher.

Van der Reijden (2020) concludes that most wave penetration is present when the wave direction is close to parallel to the channel axis. Additionally, the wave penetration is larger for small wave periods compared to the long wave periods, seen in figure 1.8a.

From the comparison of the SWAN and REFRAC model, it can be concluded that for a water level of 0 meters, the models differ the most for incoming waves from 310-360°N. However, for a water level of 2 meters, the results are comparable. It is stated that the SWAN model overestimates the critical angle for refraction by 7-16° corresponding in an overestimation of wave energy in the waves. However, the REFRAC model does not take into account the wave processes bottom friction, non-linear interaction and wave growth, while they affect the wave refraction.

Van der Reijden (2020) gives an insight in how the waves near the channel could act. Additionally, it clarifies that the SWAN model used in this thesis could give an overestimation in the amount of wave energy corresponding in an overestimation in wave heights.

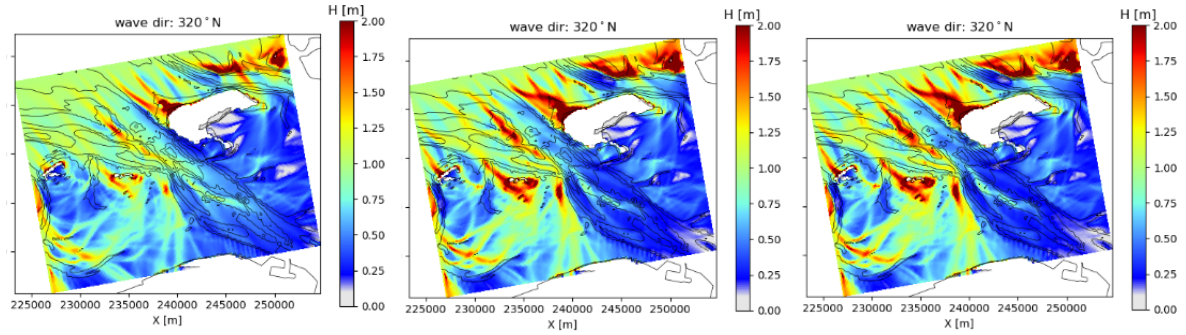

(a) Period of 5s (b) Period of 10s (c) Period of 15s

Figure 1.7: Wave heights of the SWAN model for water level at 2 meters (van der Reijden, 2020)

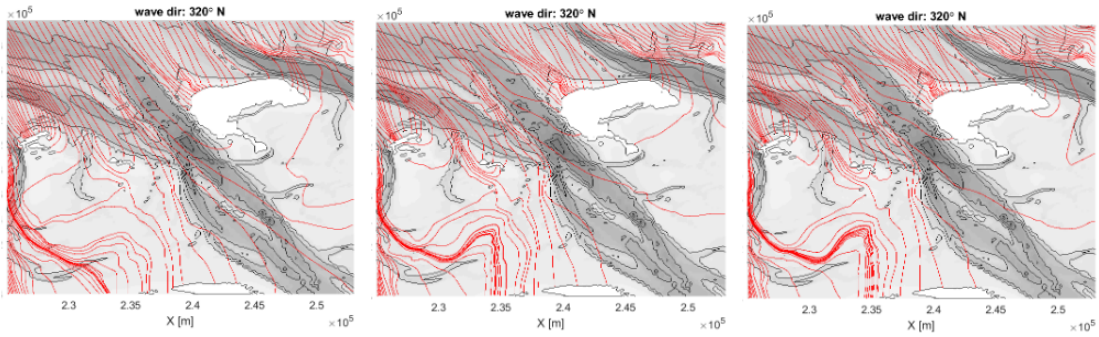

(a) Period of 5s (b) Period of 10s (c) Period of 5s

Figure 1.8: Wave heights of the REFRAC model for water level at 2 meters (van der Reijden, 2020)

1.3 Research objective and questions

The objective of this thesis is to determine the change in characteristics of waves from offshore to nearshore near the channel in the Bay of Bengal at the coast of Bangladesh. This study aims to investigate and analyse wave conditions at offshore and nearshore locations using observational and model data.

The research objective leads to the primary research question:

- How do wave characteristics change from offshore to nearshore and with respect to the channel in the Bay of Bengal near the coast of Bangladesh?

The wave characteristics will be determined based on two methods which entails two sub-questions:

1. What are the characteristics of the waves based on the measurements of the buoys?
2. What are the characteristics of the waves based on the WW3 model for offshore and SWAN model for nearshore waves?

The first sub-question will be answered by analyzing the buoys measurements data to visualise the wave characteristics. The second sub-question will be answered by understanding the wave characteristic outputs of the WW3 model and SWAN which are based on wind data sources. Once these two sub-questions are addressed and answered, a third sub-question can be formed:

3. What are the differences of wave characteristics between the measured data and the model results?

This question will describe the differences in wave characteristics between the measured data based on the buoys and the modeled characteristics based on wind data. These three sub-questions will guide the structure of this thesis, ultimately leading to the answer of he primary research question.

1.4 Thesis outline

This thesis is structured as follows:

- Chapter 2 will give relevant background information about the study area and wave theory about the wave characteristics and wave processes.
- Chapter 3 gives the results of the analysis of the wave characteristics based on the buoy measurement data.
- Chapter 4 gives the analysis results of the wave characteristics from the WW3 and SWAN models.
- Chapter 5 will compare the results of the buoy data with the WW3 and SWAN model
- Chapter 6 gives the conclusion based on the results of the different data sets and the comparison between these data sets.
- Chapter 7 will give some recommendations for future research

2 Background

This chapter presents relevant background information about what is known about the study area, as well as some theoretical background on waves. Additionally, the WW3 and SWAN models are explained.

2.1 Study area

The study area was already introduced in Figure 1.2 in the introduction. In the following sections, the bathymetry and KP locations of the channel are discussed. Additionally, the terms cyclone and depression, along with their occurrences in the study area, are discussed and the tides are discussed.

2.1.1 Bathymetry and KP locations

Figure 2.1a shows the bathymetry of the study area based on the most recent available data consisting of data from multiple years. The channel is marked by a black line, with dots spaced at 1 km intervals along its length for reference. The figure displays that even at 50 kilometer offshore, the water depths around the channel are not larger than 8 meters LAT (Lowest Astronomical Tide).

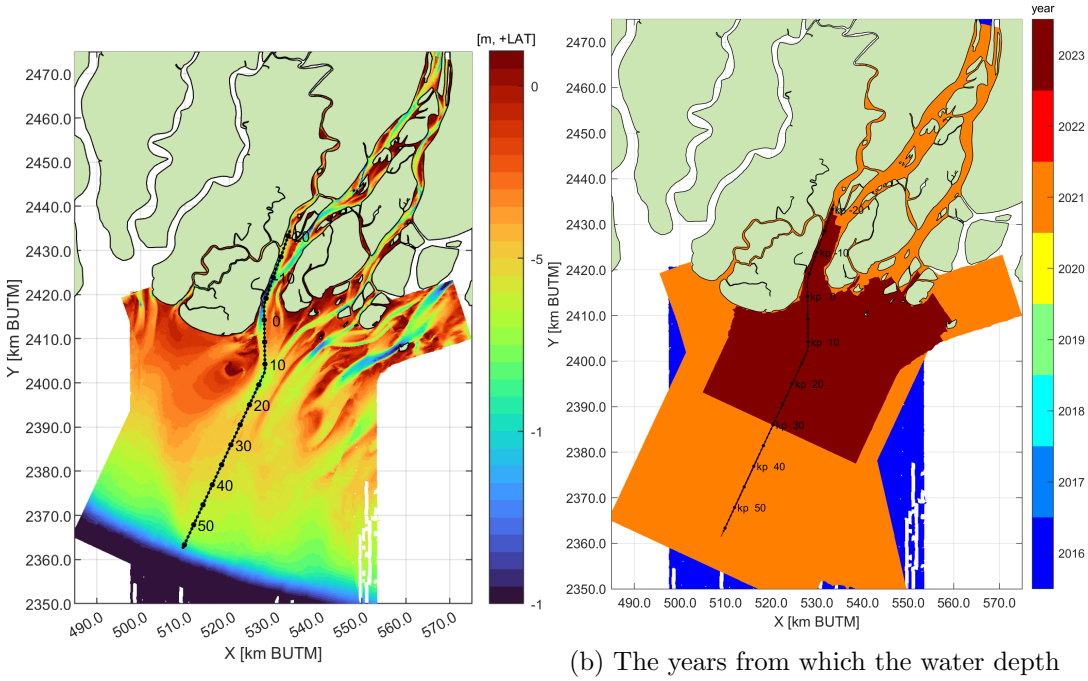

(a) The water depths expressed in m LAT

(b) The years from which the water depth data is retrieved

Figure 2.1: The bathymetry of the study area where the channel can be seen with the black line where every dot represents one kilometer

Figure 2.1b shows which bathymetry data is obtained from which year. the data collected in 2023 overlap with the collected data in 2021. The bathymetry difference between these years for the overlapping area is seen in Figure 2.2. From this figure it can be concluded that there is a significant amount of sediment transport in two years, particularly noticeable at shallow depths where the bathymetry has changed up to 5 meters. In this figure the channel can also be seen with the blue straight line, because during the period of August 2022 and April 2023

the channel has been deepened from -6.3 m LAT to -9.3 m LAT.

The channel begins 57 kilometers offshore and extends 16 kilometers inshore, where it reaches the location of the Port of Payra situated along the tributary of the channel's river. Figure 2.1a indicates that there are three general cardinal channel directions:

1. The channel direction from 57 to 12 kilometers offshore is 205 degrees.
2. The channel direction from 12 kilometer offshore to 3 kilometer inshore is 179 degrees
3. The channel direction from 3 to 20 kilometer inshore is 200 degrees.

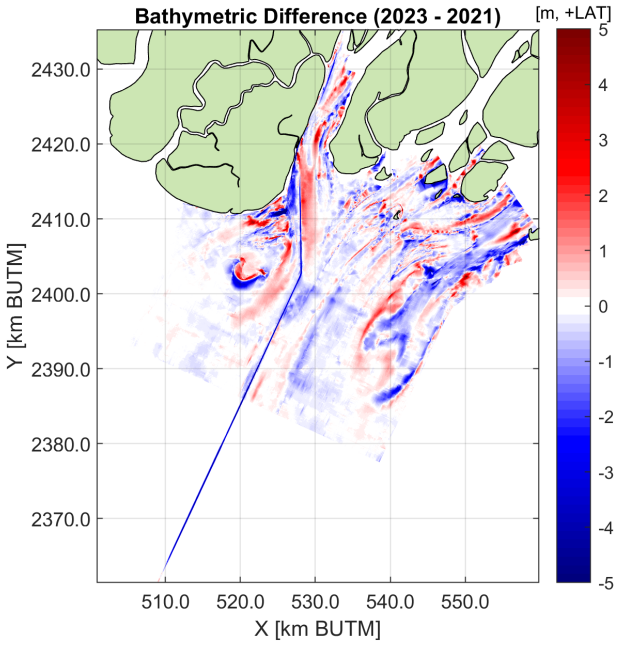

Figure 2.2: The difference in bathymetry over two years, from 2021 to 2023. Blue indicates erosion and red indicates accretion

2.1.2 Cyclones and depressions

As mentioned in the introduction, the Bay of Bengal is well-known for its cyclones. A tropical cyclone is a rapidly rotating storm system characterized by a low-pressure center, strong winds, and heavy rain. The formation of a tropical cyclone requires favorable environmental conditions: warm ocean water, atmospheric instability, high humidity, the Coriolis effect, a pre-existing weather disturbance, and low vertical wind shear (NOAA, 2023).

The process typically begins with a cluster of thunderstorms over tropical or subtropical waters with water temperatures of at least 27 degrees Celsius, often originating from tropical waves. Tropical waves are large areas of relatively low atmospheric pressure that move from east to west creating waves (NOAA, 2023).

The most important factor in the development of a tropical cyclone is warm ocean water. As water vapor rises, it cools, and condenses into liquid, forming clouds. This process releases heat, warming the atmosphere and causing the air to rise further. As this warm air rises, more air rises from below near the surface to take its place, generating the strong winds characteristic of these storms (NOAA, 2023).

When the center of the tropical cyclone, the eye, moves over land, it weakens rapidly due to the loss of its primary energy source: the moisture and heat from the ocean. Without this supply, the cyclone loses its ability to maintain the rapid rising of warm air and thunderstorms near its center, leading to a rapid decrease in strength (NOAA, 2023).

Alternatively, tropical depression is a weaker, less organized system which also bring heavy rain and thunderstorms but lack the strong winds. When the winds of a depression exceeds winds of 62 km/h it is classified as a tropical cyclone. The wind speeds of tropical cyclones can exceed up to 118 km/h (NOAA, 2023).

Cyclones and depressions registered in the Bay of Bengal

The dataset analyzed in Section 3 includes data from 2021 to 2023. The cyclones and depressions registered during this period are listed in Tables 2 and 3. The cyclones that have past near the channel are C1, C2 and C3. The cyclone C4 have passed right above the channel. The severe cyclonic storm Mandous was located far south of the coast, near the latitude of Sri Lanka and the southern tip of India. The extremely severe cyclonic storm Mocha was located east of the channel. The depressions D1, D2 and D3 passed above the channel, while D4 and D5 formed and remained far south near the same latitude as cyclone Mandous.

Table 2: The cyclones from the recent years that have past the Bay of Bengal CIMSS (2023)

	Cyclone	Year	Dates	Peak intensity (km/h)
C1	Very severe cyclonic storm Yaas	2021	May 23 - May 28	140
C2	Cyclonic storm Gulab	2021	Sept 24 - Sept 28	85
C3	Cyclonic storm Jawad	2021	Dec 2 - Dec 6	75
C4	Cyclone Sitrang	2022	Oct 22- Oct 25	85
C5	Severe cyclonic storm Mandous	2022	Dec 6 - Dec 10	95
C6	Extremely severe cyclonic storm Mocha	2023	May 9 - May 15	215

Table 3: The depressions from the recent years that have past the Bay of Bengal

	Depression	Year	Dates	Peak intensity (km/h)
D1	Deep depression BOB 03	2021	Sep 12 - Sep 15	55
D2	Depression BOB 05	2022	Aug 14 - Aug 17	45
D3	Deep depression BOB 06	2022	Aug 18 - Aug 23	55
D4	Depression BOB 10	2022	Dec 22 - Dec 27	45
D5	Depression BOB 01	2023	Jan 30 - Feb 2	45

2.2 Wave theory

A wave is a disturbance that travels through a medium, carrying energy without transferring matter. Water waves are surface disturbances in oceans caused mainly by wind energy (Basco (n.d.)). The motion of waves can be regular, described by a single representative wave height H, wave length L and wave period T. However, most ocean waves consist of multiple waves with varying heights, lengths and periods (Masselink et al., 2011).

In the ocean, waves can be categorised based on their frequencies. Figure 2.3 shows an overview of all wave types. In the Bay of Bengal, the wave types that occur are mostly wind waves and swell waves. Wind waves are generated by local winds, characterized by irregular and

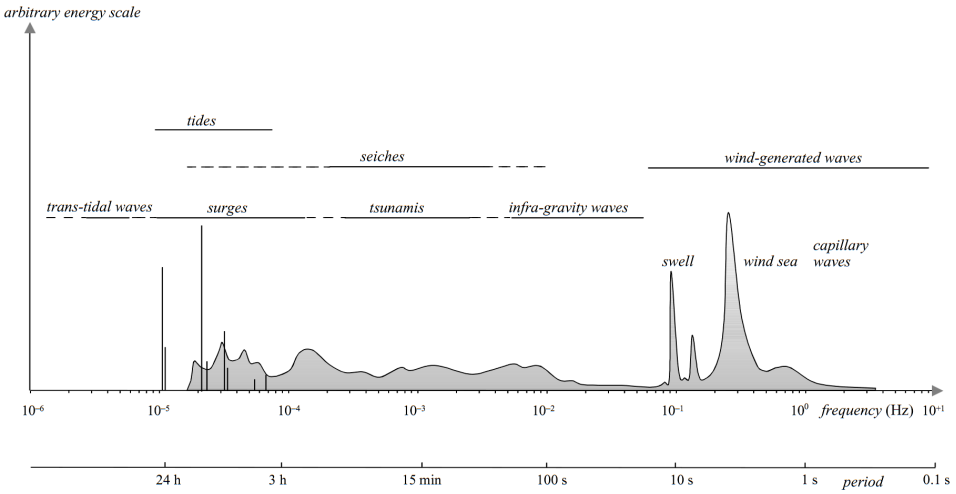

Figure 2.3: Wave types based on their frequencies and periods (Holthuijsen, 2007).

short-crested patterns. The frequency range of wind waves is between 0.1 Hz and 0.5 Hz, corresponding to wave periods of 2 to 10 seconds. On the other hand, swell waves are long-crested waves that have traveled out of their generating area. The frequency range is typically between 0.05 and 0.1 Hz, corresponding to wave periods of 10 to 20 seconds (Holthuijsen, 2007).

Tides are the type of wave motion caused by the gravitational interactions between the Earth, the Moon and the Sun. The change in the ocean water level reaches a high and low twice a day, meaning that the periods are six hours apart. The change from low to high tide is called the "flood tide" or "flow". The change from high to low tide is called the "ebb tide" (NOAA, n.d.-a).

2.2.1 Wave characteristics

There are various characteristics that can describe a wave. The wave height is defined as the vertical distance between the highest and the lowest surface elevation. The mean wave height $\overline{H}$ is defined as

$$\overline{H} = \frac{1}{N} \sum_{i=1}^{N} H_i \tag{1}$$

where N is the number of waves in the record and i the sequence number of the record. However, this definition is not very often used. The significant wave height, defined as the mean of the highest one-third of waves in the wave record. It has been shown that the value of this wave height is close to the value of the visually estimated wave height and is therefore widely used. The significant wave height can be obtained in three ways:

1. The estimated significant wave height is denoted as H_{v}.
2. The measured significant wave height is denoted as $H_{1/3}$.
3. The significant wave height estimated from the wave spectrum is denoted as $H_{\mathrm{m_0}}$ (Holthuijsen, 2007).

The measured significant wave height can be defined as

$$H_{1/3} = \frac{1}{N/3} \sum_{j=1}^{N/3} H_j \tag{2}$$

where j is the rank number of the wave, based on the wave height (i.e., $j = 1$ is the highest wave, $j = 2$ is the second-highest wave, etc.).

The wave period T is the average time interval between the start and the end of the wave. Since this wave period is defined with zero-crossings it is called the zero-crossing period, T_0 defined as

$$\overline{T}_0 = \frac{1}{N}\sum_{i=1}^{N} T_i \tag{3}$$

The wave period corresponding to the significant wave height is the mean period of the highest one-third of waves defined as

$$T_{1/3} = \frac{1}{N/3}\sum_{j=1}^{N/3} T_0, j \tag{4}$$

Additional wave characteristics are the wave frequency, which is the inverse of the wave period, the wave direction, group velocity C_g and celerity C. The wave direction is the direction from which the waves approach. The celerity is the wave velocity of one wave, whereas the group velocity is the speed at which wave groups travel (Masselink et al., 2011) with the link defined as

$$C_g = Cn \tag{5}$$

where the parameter n increases from 0.5 in deep water to 1 in shallow water.

2.2.2 Water depth classification

The waves can be categorised into three water depth types:

- Deep water: In deep water water particles under the wave move in a circular path with the diameter of the circles decreasing with an increasing water depth beneath the surface. Deep water is defined when $h/L_0 > 0.5$, where h is the water depth and L_0 is the deep water wave length.
- Intermediate water depths: At intermediate water depths, the motion of the surface waves 'feel' the presence of the bed, causing the water particles follow an elliptical path. This path becomes flatter and smaller as the seabed depth decreases. Intermediate water depths are defined for $0.05 \leq h/L_0 \leq 0.5$.
- Shallow water: In shallow water, water particles merely undergo a horizontal to-and-fro motion and are defined for $h/L_0 < 0.05$ (Masselink et al., 2011).

In the intermediate water depths and shallow waters, waves interfere with the seabed resulting in the change of wave characteristics and larger sediment transport.

2.2.3 Wave energy

The presence of waves at the water surface implies that water particles were moved from their position at rest, created by the gravitational force, to some other position. This change of position requires work done against this gravitational force which represents potential energy. In addition, the wave particles move with an orbital velocity which represents the kinetic energy Holthuijsen (2007).

According to the linear wave theory, the two forms of energy are equal and the total wave energy E is defined as

$$E = \frac{1}{8}\rho g H^2 \tag{6}$$

where ρ is the water density, g is the gravitational acceleration and H is the wave height.

The energy of waves is depended on factors such as wind strength, duration, fetch (distance over which the wind blows), water depth and wave characteristics. The wave energy increases with stronger winds, longer wind duration, and greater fetch. Steeper wind-wave interaction, especially during intensified wind events, also enhances wave energy through increased wave height and turbulence. On the other hand, wave energy decreases because of bottom frictions and during wave processes such as shoaling, wave refraction, and breaking.

The wave energy can also be represented in a two-dimensional spectrum called the variance density spectrum $E(f, \theta)$, which describes how the wave energy E is distributed over the frequency f and direction θ. The frequency spectrum $E(f)$ is the one-dimensional spectrum which shows how wave energy is distributed across different frequencies, and the directional spectrum $E(\theta)$ is the one-dimensional spectrum which shows how wave energy is distributed across different directions (Holthuijsen, 2007):

$$E(f) = \int_0^{2\pi} E(f, \theta)\, d\theta \tag{7}$$

$$E(\theta) = \int_0^{\infty} E(f, \theta)\, df \tag{8}$$

The significant wave height, H_{m_0}, can be derived from this variance density spectrum using the zero-th moment m_0, which is the integral of the frequency spectrum $E(f)$ over all frequencies:

$$m_0 = \int_0^{\infty} E(f)\, df \tag{9}$$

The significant wave height H_{m_0} is then approximated after substitutions and analytical calculations:

$$H_{m0} \approx 4\sqrt{m_0} \tag{10}$$

2.2.4 Linear wave theory

Linear wave theory, also known as the Airy wave theory, is a mathematical model used to describe the behaviour of surface gravity waves. This theory is based on the small-amplitude approximation describing the waves that are small in amplitude and their wavelength is much larger than the water depth. This theory is particularly useful for understanding the propagation of waves over long distances and in relatively deep water (Masselink et al., 2011).

Linear wave theory describes the propagation of surface waves very accurately at deep waters. However, as the waves propagate towards shallow water the small amplitude approximation is not valid anymore, leading to different results than observed waves.

2.2.5 Wave processes: shoaling, refraction and breaking

As waves propagate from deep water towards the land, they interact with the seabed and can be affected by different processes that lead to transformation of the height, length, shape, speed and direction of the wave. It is notable that the only property that remains constant as waves move to shallow water is the wave period (Davidson-Arnott, 2010).

Shoaling is the propagation of waves from deep water into decreasing water depth. When assuming no energy is loss, the wave speed C decreases as water depth decreases ($C = \sqrt{gh}$), leading to a reduction in wave length L since $C = \frac{L}{T}$. This leads to the wave height H increases as no energy is lost. Figure 2.4 shows the affect of shoaling from deep to shallow water. These

changes are most readily seen in long period swell waves which interact with the bed earliest.

In reality, as waves propagate into shallow water, energy decreases due to factors as bottom friction, wave refraction and breaking. This energy loss means that the wave height may not always increase: it can also decrease depending on specific wave dynamics and interactions.

Wave refraction describes the alignment of waves with the underwater contours as waves move into intermediate and shallow waters. This process results from the fact that wave celerity decreases as the wave shoals, meaning that the waves in deeper water will move faster than the waves in shallower water. This causes the wave crest to bend towards the alignment of the bottom contour, seen in Figure 2.5 (Davidson-Arnott, 2010).

Conservation of wave energy power is assumed during the process of wave refraction, causing an increase in wave energy where waves converge resulting in an increase in wave height and decrease in wave energy where waves divigate resulting in a decrease in wave height (Davidson-Arnott, 2010).

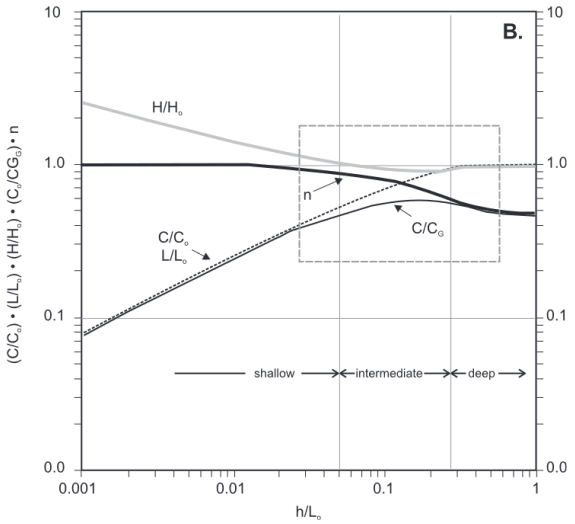

Figure 2.4: The shoaling transformation from deep to shallow water according to the linear wave theory (Davidson-Arnott, 2010).

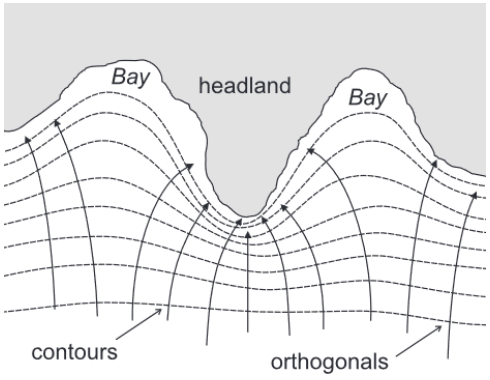

Figure 2.5: Refraction of waves as waves shoal at the coast (Davidson-Arnott, 2010).

Wave breaking occurs when horizontal water particles velocities in the wave crest exceed the velocity of the wave form. Wave breaking causes a wave energy reduction also called wave

energy dissipation (Masselink et al., 2011). In shallow water waves also break because of an increase in wave steepness caused by increase in wave height and a decrease in wave length and celerity. The breaking point of waves can be expressed based on the solitary wave theory by Munk (1949) which predicts

$$\frac{h_b}{H_b} = 1.28 \tag{11}$$

where h_b is the water depth at which breaking takes place and H_b is the wave height at breaking. From Equation 11 it can be concluded that waves begin breaking in water depths that are slightly larger than the wave height.

The three main types of breakers occurring at the coast are:

1. Spilling breakers are associated with gentle beach gradients and steep incident waves which have a large wave height relative to wave length. These waves are characterized by a gradual peaking of the wave until the crest becomes unstable, resulting in a gentle forward spilling of the crest.
2. Plunging breaks occur on steeper beaches with waves of intermediate steepness. The shore-ward face of plunging waves becomes vertical, curled over, and plunges downward and forward as an intact mass of water.
3. Surging breakers are found on steep beaches with low steepness waves where waves slide up the beach without breaking because the front face and crest of the wave remain relatively smooth (Masselink et al., 2011).

2.3 Wave Watch III and SWAN model description

The models that will be used to describe the wave characteristics are the Wave Watch III (WW3) model in the offshore areas and the SWAN model for nearshore areas.

The WW3 model is a numerical wave model used for simulating the behaviour of ocean waves which is widely used for forecasting wave conditions in oceans. This model is widely used by large-scale meteorological institutes. The model is based on meteorological data such as wind speed and direction, atmospheric pressure, and air-sea temperature differences. It also incorporates oceanographic data such as bathymetry and sea surface temperature (NOAA, n.d.-b).

The WW3 model operates by solving the wave energy balance equation, taking into account factors such as wind forcing, wave-wave interactions, and dissipation processes. It simulates the propagation and transformation of waves through various oceanic conditions, including wind-driven waves, swell, and wave breaking.

Key features of the WW3 model include its ability to predict wave heights, wave periods, wave directions, and wave spectra at specific locations and times. It can provide forecasts for both deep water and nearshore areas, making it valuable for a wide range of applications, including maritime operations, coastal engineering, and coastal management.

The engineering consultancy firm WaterProof uses the data of offshore waves retrieved from the WW3 model as input for the SWAN model to calculate nearshore waves. The SWAN (Simulating Waves Nearshore) model is a numerical wave model developed for simulating the behaviour of ocean waves in the nearshore regions. This model is also widely used by coastal engineers, researchers, and meteorologists to forecast wave conditions in coastal areas and to assess the impact of waves on coastal structures and environments. SWAN can generate one- or two-dimensional wave spectra at specified output points, while also providing spatially and

temporally varying distributions of key parameters such as significant wave height, various wave periods, wave direction, and directional spreading (SourceForge, n.d.).

3 Results: Wave characteristics based on buoys

This section provides the results of the wave characteristics based of the buoy measurement dataset to answer the first sub-question: What are the characteristics of the waves based on the measurements of the buoys?

3.1 Data availability of buoys

The first analysis of describing the wave characteristics is based on measured data from buoys. During the time period from May 2021 to July 2023, buoys positioned at various locations in the channel have captured and measured wave characteristics. These locations are denoted using KP (Kilometre Point) notation, consisting of a numerical value indicating the kilometre point along with for some points an additional letter to indicate the cardinal direction relative to the channel. Figure 3.1 visualises when data is available for each KP location. For these periods for each KP location the buoys have recorded wave data for every 30 minutes. Figure 3.1 also shows the cyclones and depressions registered during the time period. Additionally, there are two overlap periods of KP locations far apart from each other. The wave characteristics of these time instances will be compared and are called overlap period A and B, highlighted in light blue. The overlap period C, D, E and F represent the period for which data is provided for the same KP location, but different cardinal direction. All overlap periods will be discussed in the next Section.

The buoys have captured various wave parameters, including the significant and mean wave height, the peak and mean period, the peak and mean direction and the directional spread. From Appendix B it can be concluded that KP locations -19.5W and 22E are not considered in the analysis because the time period of these points are to small to draw conclusions.

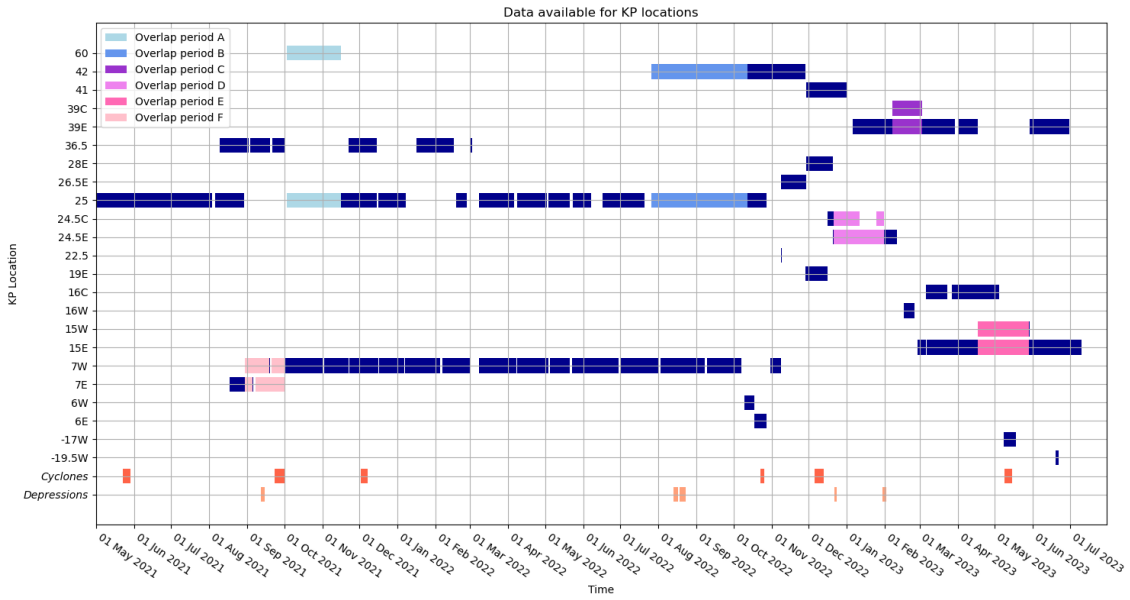

Figure 3.1: The time period for which the buoys have captured wave characteristics. The overlap periods are the periods for which the data will be compared. The cyclones and depressions registred during this time period are plotted at the bottom.

3.2 Bathymetry at buoy locations

The bathymetry influences the wave characteristics at sea. Therefore, knowing the bathymetry around the channel and the water depths of the KP buoy locations is helpful for understanding the data output. Figure 3.2 displays the coordinates of the KP locations along with the water depths in meters LAT. The figure visualises whether the KP locations are situated to the east, west or center of the channel. Moreover, this figure shows that at KP locations far from the coast, the water depth is not lower than 10 m LAT, except at KP60. The bathymetry data of Figure 3.2 is partly from 2023 and partly from 2021, together representing the most recent bathymetry data available for the area.

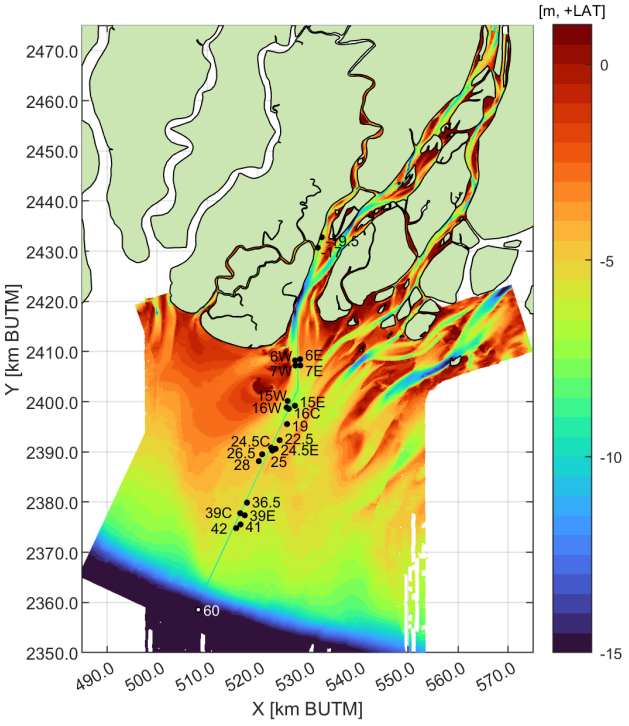

Figure 3.2: Most recent bathymetry of the study area with all KP locations where buoys have measured wave characteristics.

Variations in water depth can have influence on the wave characteristics and it should therefore be considered when analysing at the buoy data. Appendix C provides the water depths of the KP locations for 2021 and 2023. For the KP locations 39C, 24.5C, 16C, 15E, 15W, 7E, 6E, 6W and -17W there is a significant difference indicated in red. The buoy data from KP-17.5W and 7E has been captured outside the period of the channel deepening, but for the other locations the data is in between or overlapping the time period. This should be accounted for when analysing the buoy data.

3.3 Data analysis

3.3.1 Significant wave height

The buoys have directly measured the significant wave height $H_{1/3}$ at the KP locations. The significant wave height for KP25 have been captured for more than one year. Figure 3.3 shows higher significant wave heights during the months June up until September, representing the monsoon. In addition, at some time instances high peak values are seen. These could be

explained based on cyclones. This possible relation will be discussed in paragraph 3.3.3 where cyclones are discussed. For the KP location 7W data is also available for over a year. As shown in Figure 3.4, the monsoon period is indicated by an increase in wave height. From Appendix G.1 it can be concluded that for the datasets of KP25 and KP7W, the significant wave height at 7W is everywhere consistently lower.

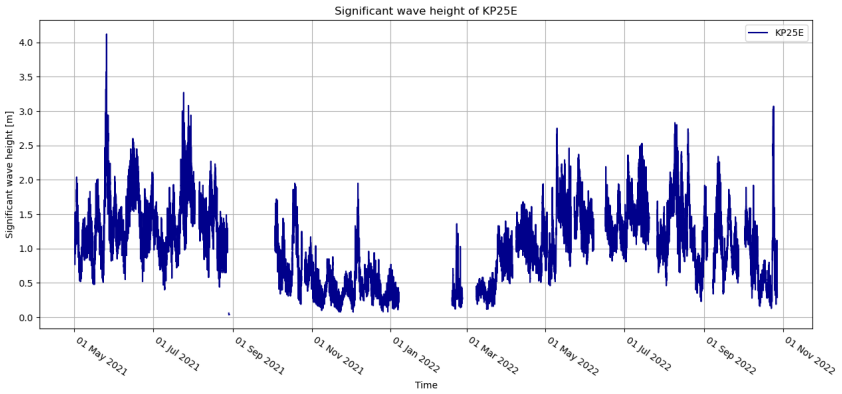

Figure 3.3: Time series of the significant wave height for KP25

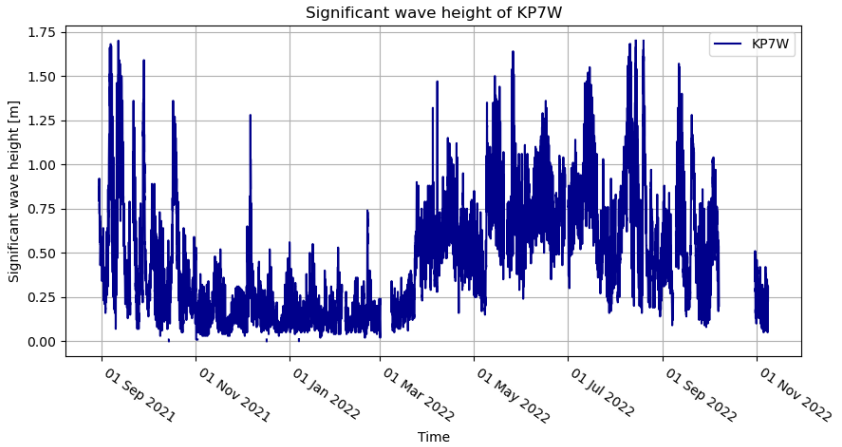

Figure 3.4: Time series of the significant wave height for KP7W

When plotting KP locations far offshore within a single figure, the entire dataset can be represented in terms of significant wave height. Figure 3.5 illustrates that during each monsoon season, the significant wave heights are notably higher compared to the other months. Additionally, the figure shows that during periods when multiple KP locations have recorded data, those closer to the coast have slightly lower significant wave heights.

The significant wave heights of the other KP locations can be found in Appendix F, where the cyclones have also been plotted in the figures. From the figures, it can be concluded that when the significant wave height increases beyond that caused by tidal changes, this increased wave height typically lasts for five days. Higher significant wave heights indicate more energy in the waves coming from stronger winds or waves origination from far away. In the extreme cases, when these winds are very strong, cyclones are formed resulting in very high significant wave heights. The cyclones will be discussed in paragraph 3.3.3.

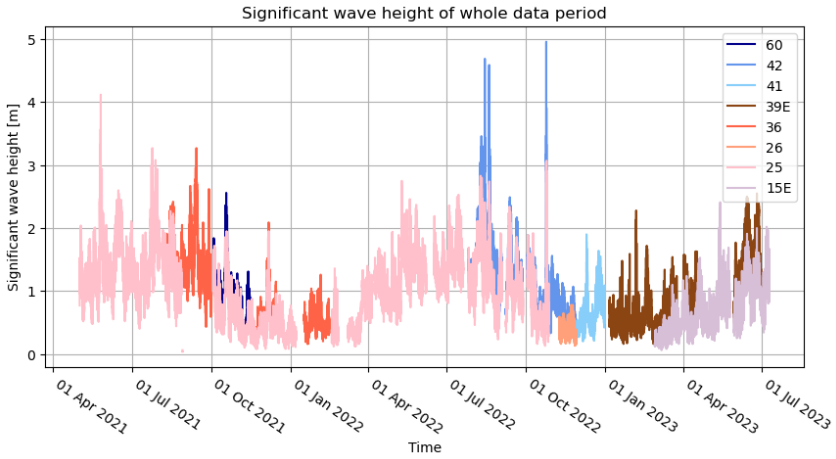

Figure 3.5: The significant wave height for the buoy measurement time period for the KP location 60, 42, 41, 39E, 36, 25 and 15E.

3.3.2 Comparison between locations

At various time intervals, multiple buoys have captured data at different KP locations. To visualise the change in significant wave height from farther away to closer to the coast, figures have been plotted showing the significant wave height at multiple KP locations.

Comparison between KP locations

Figures 3.6 and 3.7 show the significant wave heights during overlap period A and B, respectively, as indicated in Figure 3.1. The figures show that a fluctuation in wave height is measured at all locations and KP25 and KP7W consistently have lower wave heights than KP60 and KP42. Although KP60 and KP42 do not have data for the same time frame, the figures indicate that the blue line for both locations have the same height difference compared to KP25. This suggests that the significant wave height at KP60 and KP42 is similar, with no significant decrease in wave height between these two locations. The water depths at KP60 and KP42 are -17.52 and -7.58 m LAT respectively indicating that the waves are barely affected by the seabed at KP42, as the significant wave height did not decrease.

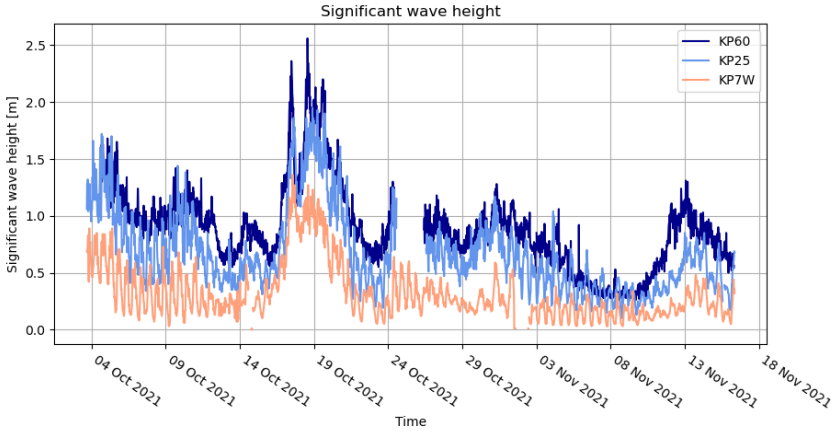

Figure 3.6: Time series of overlap period A, indicated in Fig.3.1 where the significant wave height of KP60, 25 and 7W can be seen.

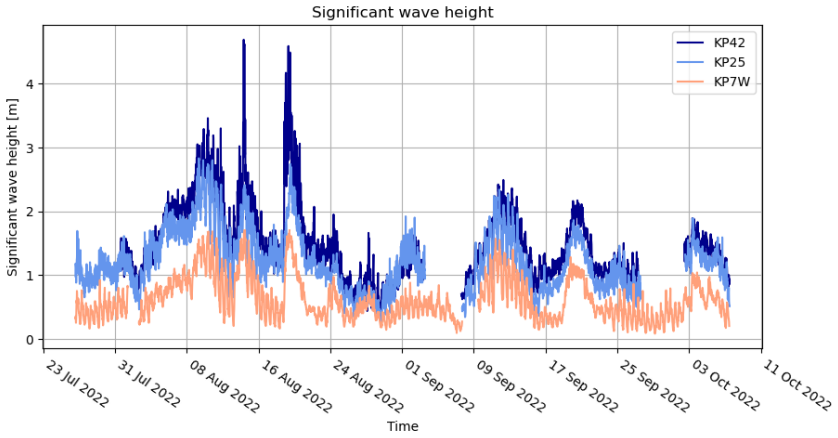

Figure 3.7: Time series of overlap period B where the significant wave height of KP42, 25 and 7W can be seen.

Comparison of KPs far from the coast

Figure 3.8 displays the significant wave height for the KP locations far away from the coast for two years where the two years have been plotted over the same months. In Table 4 in Appendix C the water depths of KP42, 41, 39E and 36.5 can be found, all approximately around -7.40 m LAT. The figure shows that for these KP locations the significant wave height remains similar, reinforcing the fact that wave characteristics are minimally influenced by the seabed until depths of -7.40 m LAT. In Figure E.1 in appendix E the KP locations 36.5E, 28E and 25E have also been plotted. From this figure, it can be concluded that the significant wave height is lower at these points, indicating that the seabed has a significant influence on the wave height.

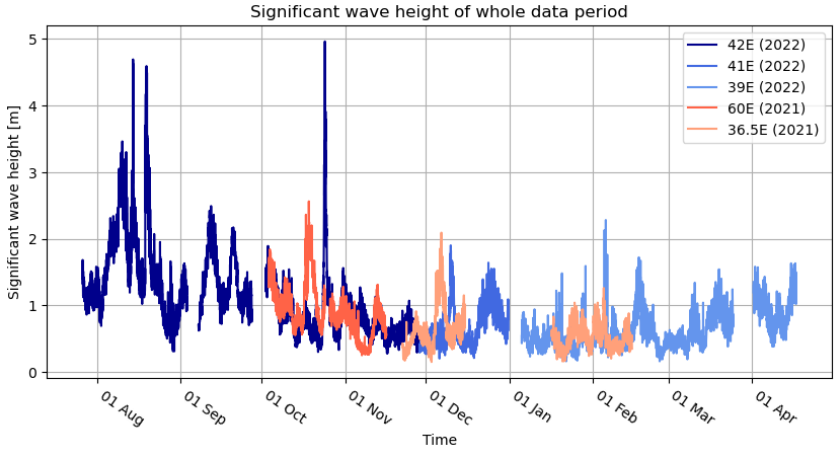

Figure 3.8: Time series of one year where the significant wave height of the KP locations 42, 41, 39E, 60 and 36.5 have been plotted without the year of which the data is retrieved.

Comparison of KPs with same KP, different cardinal direction

The dataset also has data for the same KP value but different cardinal direction. The cardinal directions are indicated with the letters C, E or W corresponding to center, east or west related to the channel. Comparing these values shows the impact of the channel on the significant wave height. Figure 3.9 shows the significant wave height of overlap period C, corresponding to KP 39E and 39C. Additionally, the direction relative to the channel is seen. The positive degrees correspond to wave directions coming from the west of the channel and negative degrees correspond to wave directions coming from the east of the channel. This figure shows that the

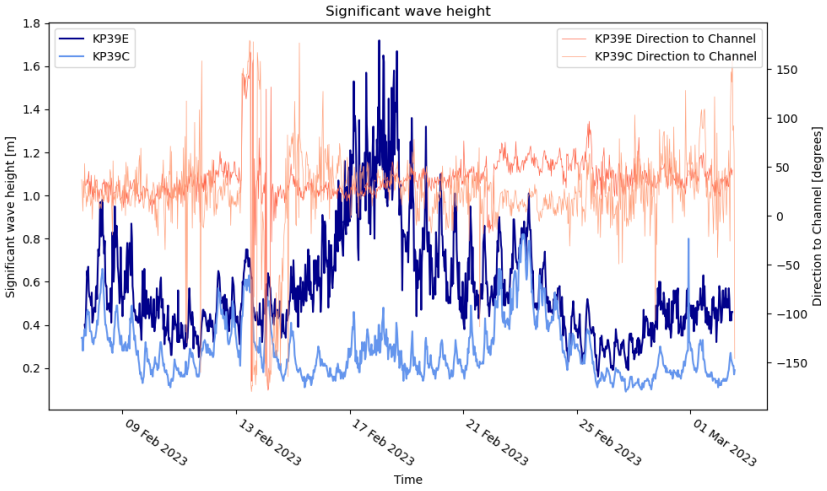

Figure 3.9: The significant wave height (blue, left axis) and wave direction (orange, right axis) of the overlap period C of Fig.3.1 corresponding to locations KP39E and KP39C.

peak significant wave height around 18 February 2023 is not captured in the channel at 39C and the significant wave height of 39C is consistently lower than 39E. According to the principle of wave power conservation, as described by the equation 6 in chapter 2.2.3, the significant wave height decreases as the water depth increases. In the channel, the water depth is larger, leading to this decrease in wave height.

From Appendix G.2, it can be concluded that at KP24 the significant wave height is also lower in the channel than at 24E. However, when the wave direction shifts to approximately 180 degrees from the channel, the significant wave heights between the locations are nearly the same. In addition, for KP15 and KP7, the data shows that the significant wave heights on the east and west sides of the channel are almost identical, with the wave direction nearly parallel to the channel. This indicates that at these points the channel has minimal effect on the wave height.

3.3.3 Effects of cyclones and depressions

In the previous paragraph, the significant wave heights for KP locations were compared. However, the peak values in these graphs have not yet been discussed. These peaks will be analyzed based on the cyclones and depressions that have been recorded. The cyclones and depressions recorded during the time period have been discussed in 2.1.2.

Figure 3.10 shows all cyclones and depressions captured during the time frame of the buoy dataset. The dark blue line represents all values of the measured significant wave height from KP60 to KP25. In appendix F all cyclones and depressions are shown for each KP location individually. Analysis of these figures, along with figure 3.10, reveals that cyclones Yaas en Sitrang and depressions BOB05 and BOB06 recorded the highest significant wave heights. Despite depressions typically associated with lower wind speeds, these two depressions together with BOB03 occurred very close to the channel causing in relatively high peak values of the significant wave heights. This is why the wave heights for BOB03 are higher than for the cyclone Gulab.

Cyclone Jawad, occurring in December, captured exceptionally high peak values compared to the surrounding values of this cyclonic event. Despite cyclone Jawad's absolute peak value being lower than that of cyclone Gulab, the increase in wave height relative to the wave height

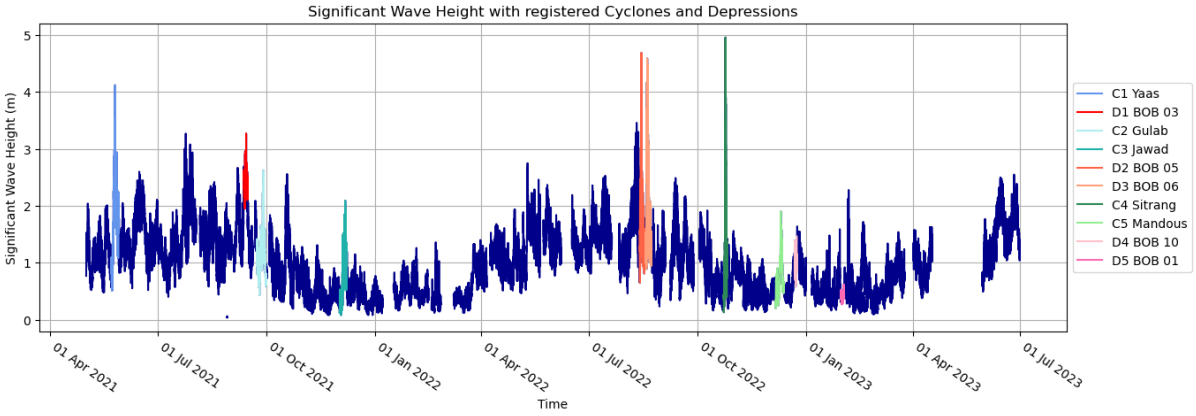

Figure 3.10: The cyclones and depressions recorded during the time period of buoy measurements. The dark blue line are the measured significant wave heights of the KP locations 60, 42, 41, 39E, 39C, 36, 26, 25 and 15E.

values around the cyclone is higher. The severe cyclone Mocha originated far south of the Bay of Bengal, resulting in its peak value being less significant compared to other storms.

The depressions BOB10 and BOB01 were situated far south of the coast, near the latitude of Sri Lanka and the southern tip of India. Consequently, the peak values associated with these depressions are not notably high, as seen in figure 3.10.

Besides the registered cyclones and depressions, other higher peak values in the significant wave height are observed in Figure 3.10, for instance at 23 July 2021. These peaks could result from strong winds that are not intense enough to form a depression or cyclone. Alternatively, they could be caused by winds originating far south, resulting in a long fetch. In addition, if these winds last for a longer period, they can also generate high waves.

3.3.4 Wave directions

In Section 3.3.2 the wave directions were already addressed when comparing the KP locations of the same value regarding the difference in wave height. In this paragraph, the direction will be identified for all KPs to draw conclusions about the direction and change in direction when waves propagate towards the coast.

Figure 3.11 shows the significant wave height and wave direction of KP16W. The wave direction fluctuates around the channel direction, where positive degrees indicating waves coming from west of the channel and negative degrees indicating waves coming from the east. Appendix H contains the wave directions for all KP locations. It can be concluded that at all locations, the wave direction fluctuate around the channel. Even when the channel rotates after KP12 from 205 to 179 degrees and after KP-3 from 179 to 198 degrees, the wave direction still fluctuates around the channel. This indicates that wave directions near the channel change according to the channel direction, likely due to wave refraction.
Appendix also shows that at many locations, there are instances where wave direction fluctuates from above 170 degrees to below -170 degrees, as seen in Figure 3.12. On possible reason for these fluctuations is that the buoys may not measure wave direction accurately when significant wave heights are low. However, these fluctuations also occur at higher significant wave heights. It is possible that river water discharge into the sea causes the wave direction to reverse in the absence of extreme weather conditions. However, this also occurs at locations far from river outlets, suggesting that these fluctuations might be measurement errors from the buoys.

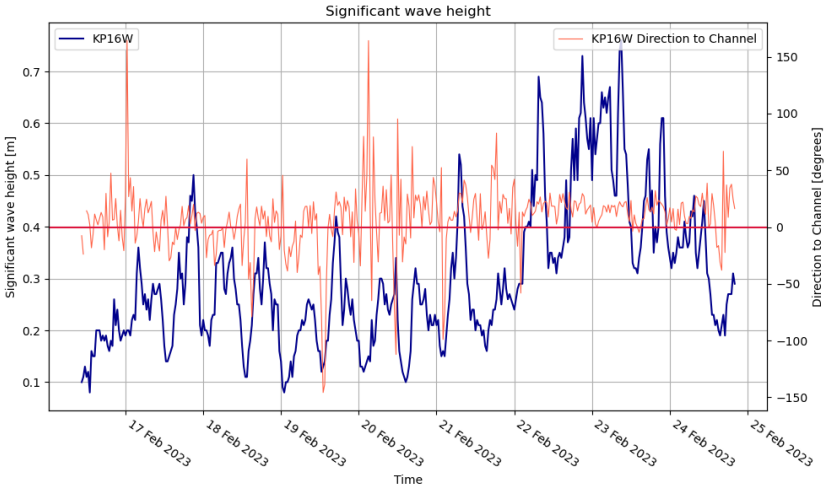

Figure 3.11: The significant wave height (blue, left axis) and wave direction (orange, right axis) of KP16W.

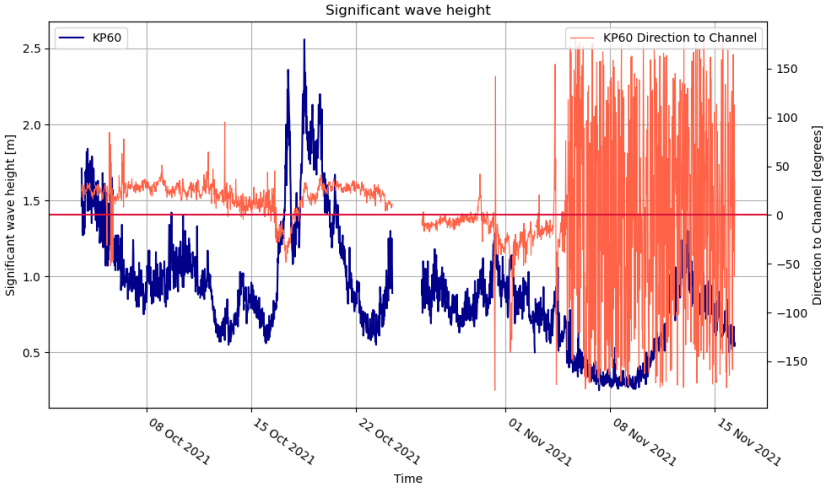

Figure 3.12: The significant wave height (blue, left axis) and wave direction (orange, right axis) of KP60.

3.4 Conclusion

In this chapter, the wave characteristics based on data from buoys located across various KP locations near the channel have been analysed. The focus of data analysis of the wave characteristics was on the significant wave heights and the mean directions of the waves.

The analysis of significant wave heights reveals that wave height decreases as waves propagate towards the coast. At KP28E the significant wave height has decreased significantly in comparison with the KP locations further away, which indicates that the waves are from this point affected by the seabed. Consequently, as waves propagate towards the coast, the waves are increasingly affected by the seabed, resulting in more sediment transport near by the coastline.

During the monsoon period, significant wave heights are notably higher compared to other periods. Cyclones and depressions recorded in the area account for most of the higher wave height values. For higher values where no cyclone or depression was registered, the cause could be

winds originating from the far south and winds that last for an extended period. Additionally, these peaks could be caused by strong winds, but they did not meet the criteria to be classified as a depression or cyclone.

In most cases, the wave direction fluctuated around the channel at all locations, even when the channel's orientation changes, due to wave refraction. However, there are instances where wave directions reverses by 180 degrees. This change could be water discharging from the river upstream to the ocean, but these fluctuations could also be errors from the buoys.

4 Results: Wave characteristics based on wave models

This section provides the results of the wave characteristics of the WW3 and the SWAN model to answer the second sub-question: What are the characteristics of the waves based on the WW3 model for offshore and SWAN model for nearshore waves?

4.1 Wave characteristics based on the WW3 model

4.1.1 Data description

The model provides wave characteristic outputs at the location of 21°00'N latitude and 90°00'E longitude. Translating this to the BUTM coordinate system corresponds to the point shown in Figure 4.1 with the label WW3 (EPSG, n.d.). In this figure the buoy KP locations are also displayed, to visualise how this points relates to the KP locations. The WW3 point corresponds to a water depth of 69 m MSL.

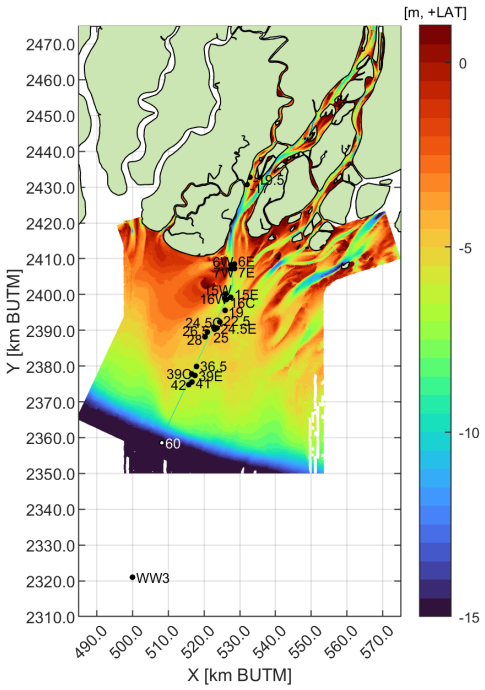

Figure 4.1: The bathymetry of the study area with the WW3 point to indicate where this point is located relative to the other KP locations.

The dataset spans from January 9, 1979, to May 31, 2024, with data captured every 3 hours. It contains a 2D spectral energy density, which describes how the variance of sea surface elevation is distributed over spectral frequency and direction. This means that for each 3-hour interval in the dataset, the energy density (expressed in m^2/Hz/rad) is defined based on spectral frequencies and directions. There are 35 spectral frequencies, equally distributed on a logarithmic axis between 0.0345 and 0.8827 Hz, and 36 spectral directions, centered in 10-degree wide bins, expressed in radians.

The 2D spectral energy density can be translated into a 1D directional spectrum, $E(\theta)$, by integrating over the frequencies, resulting in the energy distribution across each direction bin for the time period. Similarly, it can be translated into a 1D frequency spectrum, $E(f)$, by integrating over the directions, resulting in the energy distribution across the frequency for the time period. Using the theory discussed in Section 2.2.3, the 1D frequency spectrum can be translated to

determine the significant wave height H_{m_0} for each time step. Hence, the significant wave height is estimated from the wave spectrum, which differs from the measured significant wave height used in Chapter 3. To compare this dataset with the buoy data, the same time range has been used for the comparison in Chapter 5, covering May 2021 to August 2023.

4.1.2 Results

The 1D frequency spectrum, 1D directional spectrum and significant wave height H_{m_0} are shown in Figures 4.2a, 4.2b and 4.3, respectively. Figures 4.2a and 4.2b show that the total wave energy is higher during the monsoon season (June to October) compared to other months. This increase in energy corresponds to higher significant wave heights, seen in Figure 4.3.

For the 1D frequency spectrum, the frequencies range from approximately 0.05 Hz to 0.32 Hz, representing both swell and wind waves. During the monsoon season, the frequencies are widely distributed, representing both swell and wind waves present. Alternatively, during the non-monsoon months, the sea primarily consists of swell waves.

For the 1D directional spectrum, the wave direction remains relatively constant over the years, with a slight deviation from the average direction of 198 degrees (South-southwest) during the monsoon seasons. The dotted red line indicates the channel orientation, which is slightly more westward.

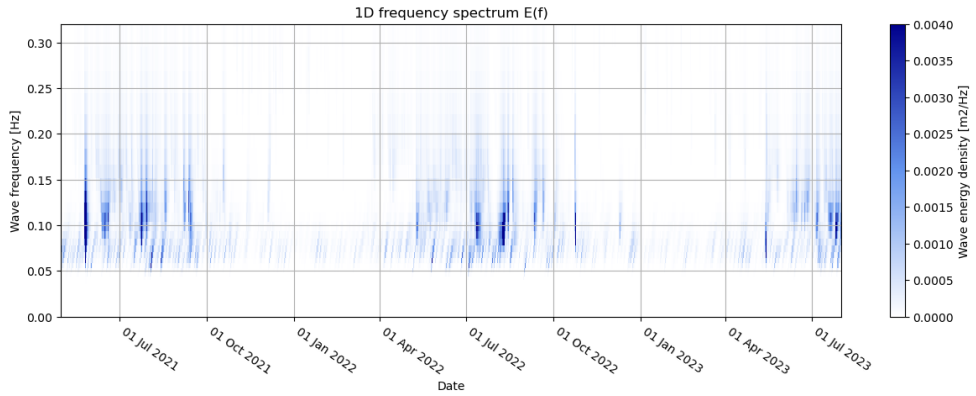

(a) 1D frequency spectrum $E(f)$.

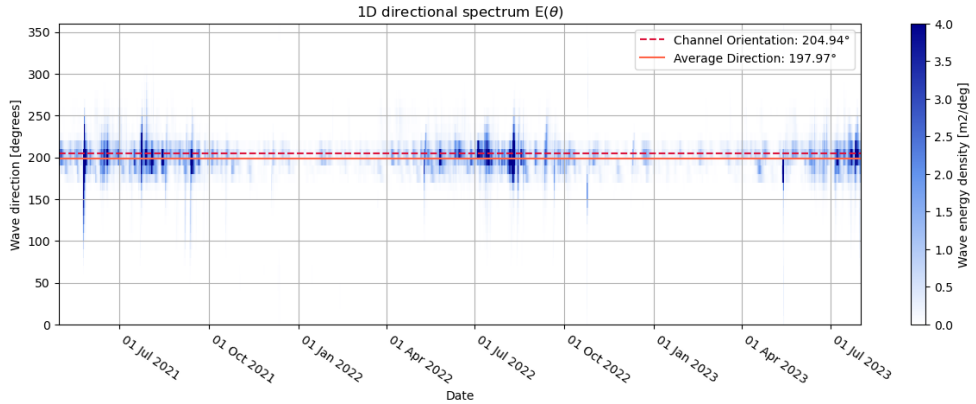

(b) 1D direction spectrum $E(\theta)$.

Figure 4.2: The 1D energy density spectra of the WW3 model for the buoy measurement period.

Figure 4.3 shows the significant wave height H_{m_0} for the measurement period with the registered cyclones and depressions. The figure shows that all peaks are explained based on a cyclones or depression, except for the peak on July 23, 2021.
Appendix I also shows the figures for the 1D frequency and directional spectrum and significant wave height for the entire dataset from 1979 to 2024. These figures also indicate that the total energy in consistently higher during monsoons, corresponding in higher significant wave heights. The frequencies range between 0.05 Hz and 0.32 Hz, representing a mix of swell and wind waves during the monsoon season and primarily swell waves during the non-monsoon season. The average wave direction for the entire dataset is 200.69 degrees, differing by 2.73 degrees from the overlapping dataset. The significant wave height for the entire dataset shows during every monsoon period higher wave heights with an average height between approximately 2 and 4 meters. The peak from May 20, 2020, corresponds to the super cyclonic storm Amphan, where the significant wave height reached 11 meters (CIMSS, 2023).

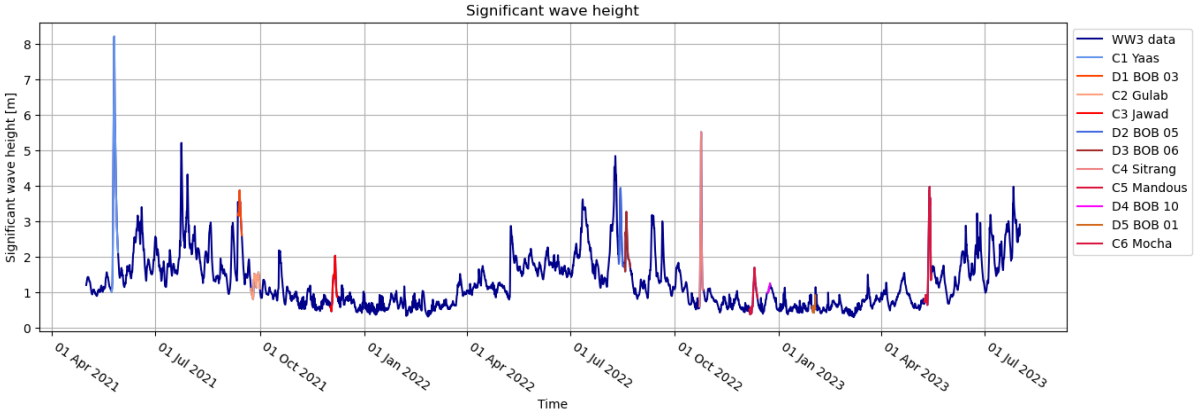

Figure 4.3: The significant wave height H_{m_0} of the WW3 model for the buoy measurement period.

4.2 Wave characteristics based on the SWAN model

4.2.1 Data description

The SWAN model provides significant wave heights and wave directions for the grid shown in Figure 4.4. This figure displays the KP locations and the WW3 point for reference. In this figure, the WW3 point appears slightly of the grid, but in the dataset, the coordinates of the WW3 point contain wave characteristic values. The SWAN model covers a short period from 1 August 2021 to 30 September 2021, with data captured every 1 hour. During this period, Cyclonic storm Gulab was registered.

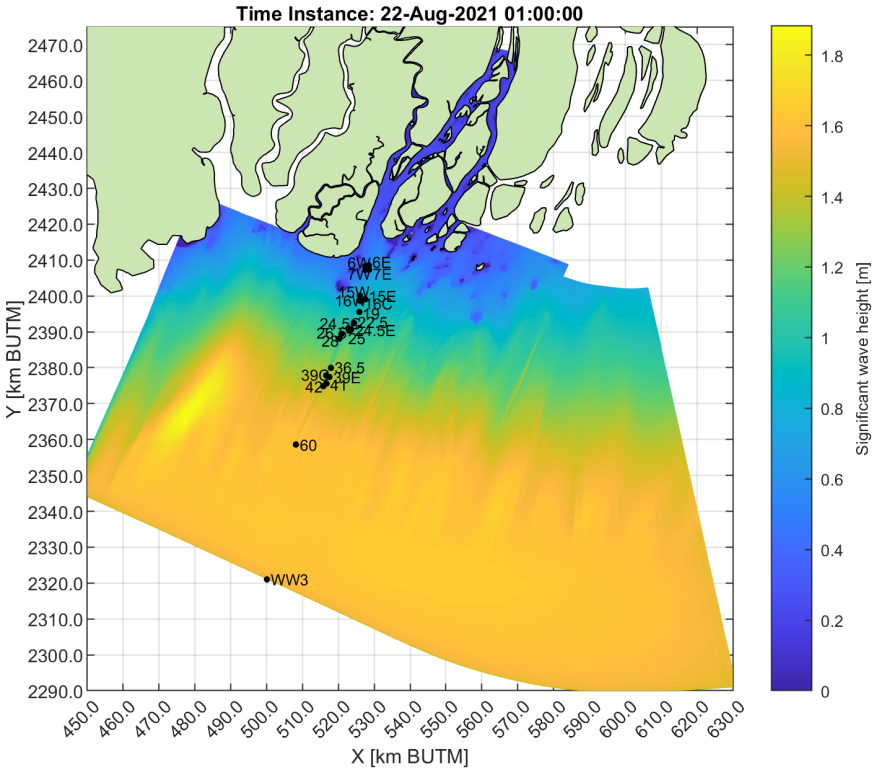

Figure 4.4: A snapshot of the SWAN model grid

4.2.2 Results

The results of the SWAN model are figures such as Figure 4.4, which show the significant wave height across the entire grid. To compare this dataset with buoy measurements and the WW3 model point, the significant wave heights at the KP locations and the WW3 point are retrieved for each time step.

Figure 4.5 shows the significant wave heights at all locations over the entire time period. It shows that significant wave height decreases as the waves propagate towards the coast, with the highest significant wave heights captured on 13 September 2021 at 3:00 for all locations. The figure also indicates that the significant wave height differences between the locations, except for WW3 and KP60, are minimal, and tidal patterns are clearly visible at these points. The WW3 and KP60 locations are hardly affected by the tides and on the peak time instance, the wave heights are significantly higher than the other locations.

Figure 4.6 shows the grid for an average time instance and for a peak time instance. Figure 4.6b shows that the significant wave height rapidly decreases after KP60, which is right after the point where the water depth decreases significantly with around 10 meters. Figure 4.6a represents an average significant wave height. The significant wave height decreases less rapidly and that the significant wave height decreases significantly after KP60. Additionally, the figure shows that the wave heights in the channel is lower, and that on the East side the wave heights remain longer higher.

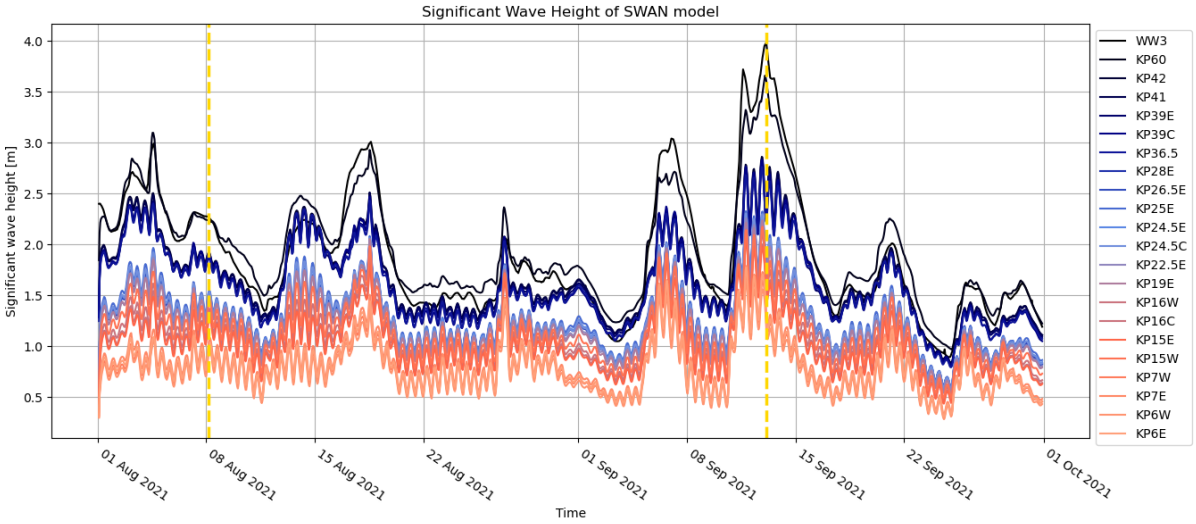

Figure 4.5: The significant wave height of the SWAN model for every location with two yellow dotted lines representing the time instances for Fig.4.6

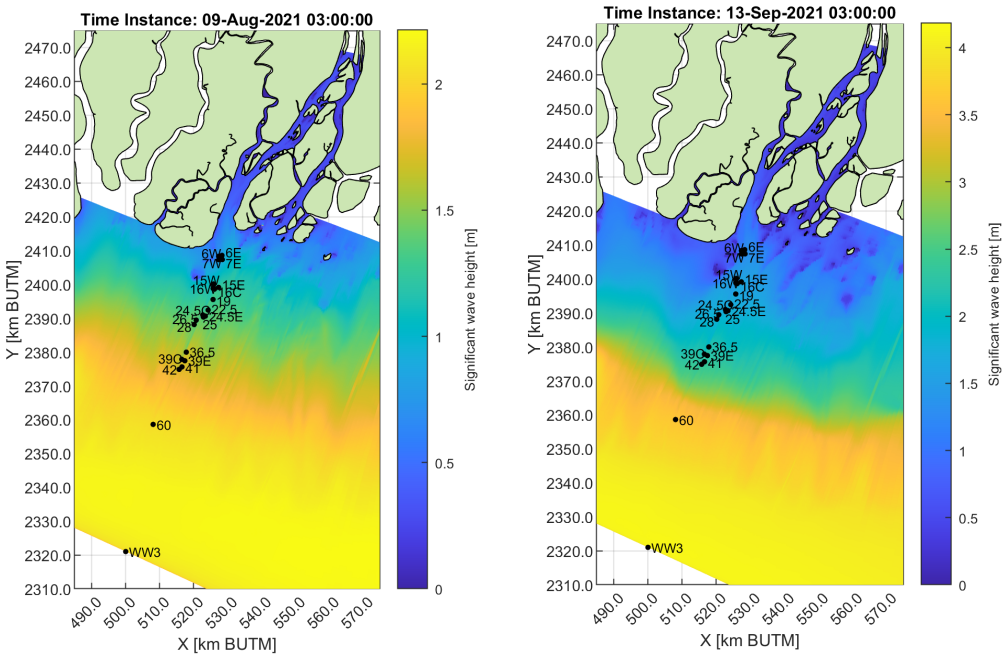

(a) Average time: 9 August 2021 at 3:00 (b) Peak time: 13 September 2021 at 3:00

Figure 4.6: The modeled significant wave height H_v of the SWAN model at two time instances

Figure 4.7 shows the wave direction for all locations. It can be seen that the wave direction is almost identical for every direction. When the channel orientation changes after KP12, the wave directions of KP7 and KP6 are hardly changed according to the SWAN model. The wave directions fluctuate around the 200 degrees with outliers above and below this direction.

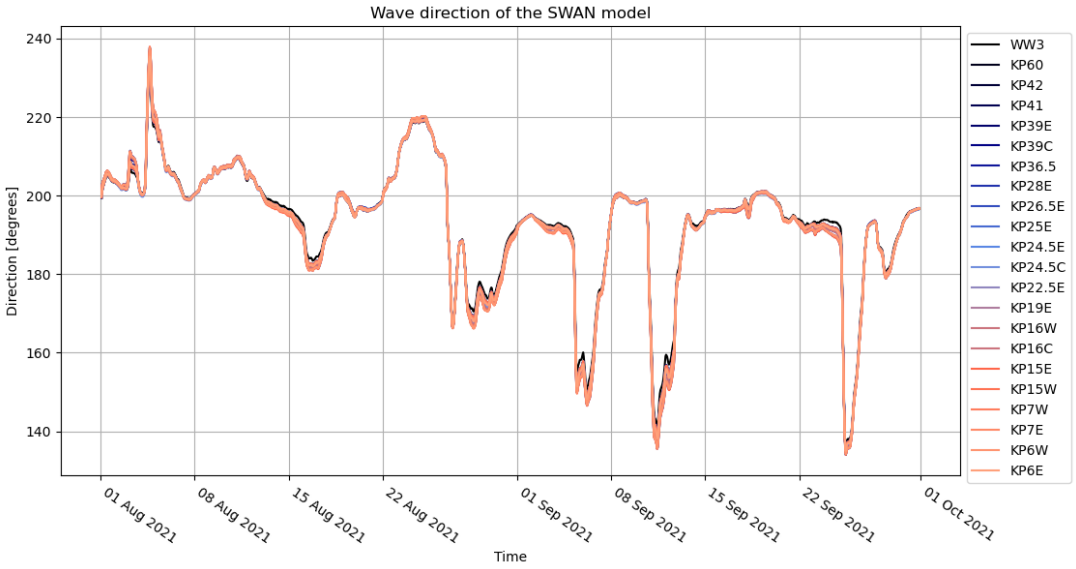

Figure 4.7: The wave direction of the SWAN model for every location

5 Discussion: Comparison between buoy measurements and wave models

This chapter compares the significant wave height and wave directions of the different datasets analysed in the previous two chapters. It will answer the third sub-question: What are the differences of wave characteristics between the measured data and the model results?

5.1 Water depth approximations at KP locations

Section 2.2.2 discusses that wave characteristics are affected by the seabed in intermediate depths and shallow waters. These depths can be determined based on the h/L_0 condition, where h represents the water depth at the specific location of interest and L_0 represents the wave length in deep water.

The WW3 point is the most far location from the coast at which data is available. The water depth at this point is 69 meter with respect to the mean sea level. At this location the L_0 has been calculated to identify whether this WW3 location can be considered as deep water. Appendix J concludes that the WW3 location can be considered as deep water, while all KP locations are classified as intermediate and shallow water. This means that at these locations the wave characteristics are affected by the seabed.

5.2 Comparison of buoy measurements with the WW3 model

The significant wave height obtained from the energy wave spectrum of the WW3 point can be compared with the significant wave heights of the buoy measurements. Figure 5.1 shows the significant wave heights for the WW3 point and the KP locations relatively far away from the coast. The figure shows that the significant wave height of the WW3 point are on the upper edge of the measured heights.

Appendix K.1 shows that as the waves propagate towards the coast, the difference between the WW3 point and the KP locations increases. Furthermore, the peak values captured by the KP locations are also seen at WW3.

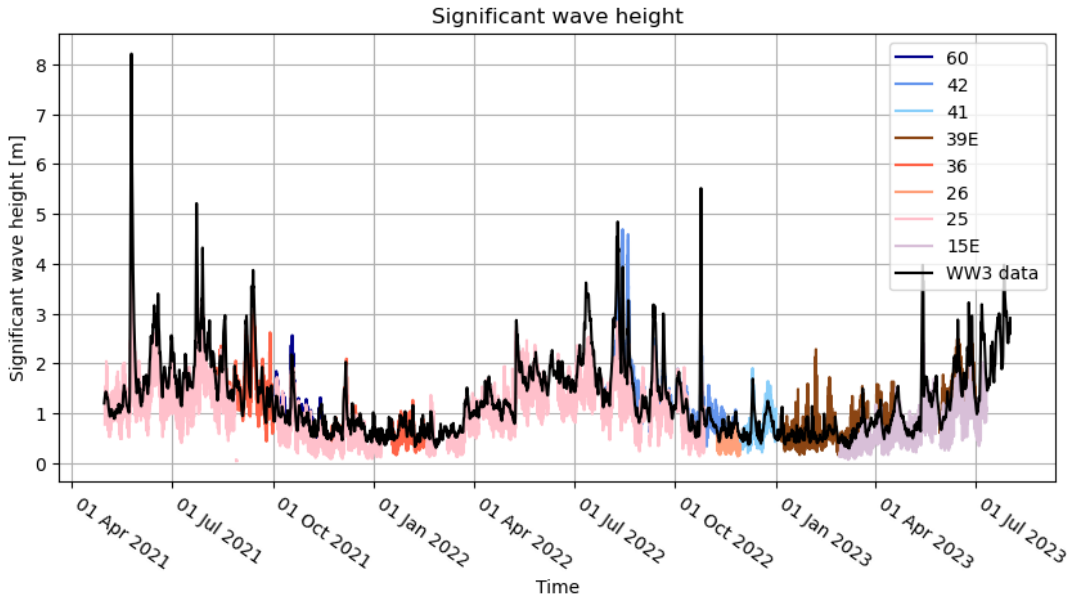

Figure 5.1: Time series of the significant wave height of the point WW3 together with the wave height of the buoy measurements from KP60 to KP15E

The wave direction of WW3, as discussed in Section 4.1.2, has an average direction of 198 degrees, which is close to the channel orientation of 205 degrees. Section 3.3.4 showed that the wave directions of all KP locations were also very close the the channel orientation. This suggest that the wave direction between the WW3 point and KP locations are very similar. Additionally, Figure 5.2 in Appendix K.1 also shows that the wave direction from KP25 measured by the buoy is very similar to the modelled wave directions form the WW3 model.

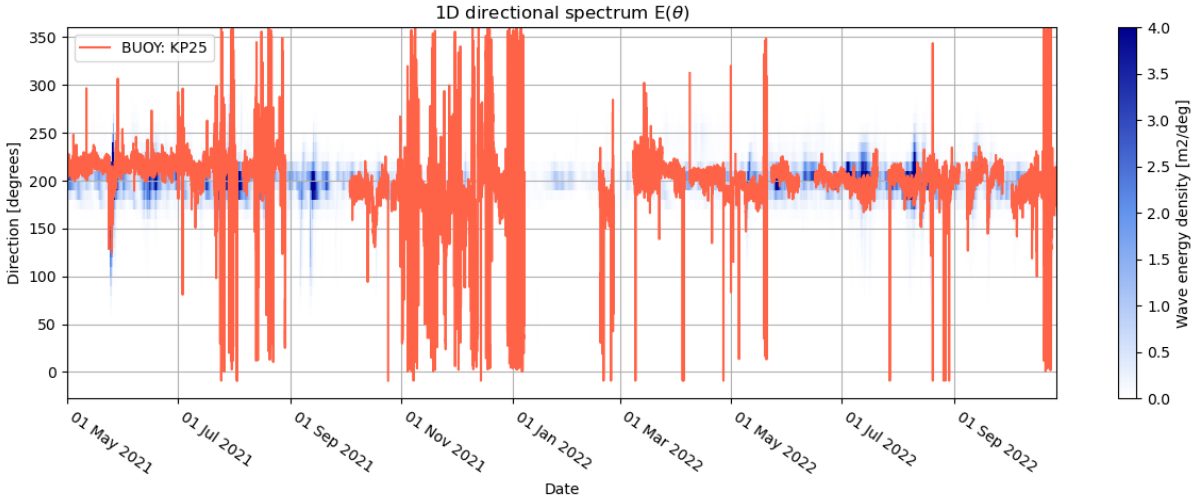

Figure 5.2: Time series of the wave direction of the WW3 point according to the WW3 model and the wave direction of KP25 measured from the buoy.

5.3 Comparison of buoy measurements with the SWAN model

A comparison between datasets is only valid when the datasets have the same time interval. Otherwise, it is unclear if the environmental conditions are constant, such as wind direction and speed. There are four locations, KP36.5, KP25, KP7E and K7W, that have overlapping time intervals between buoy measurements and the SWAN model.

Figure 5.3 shows the significant wave height for both datasets of KP36, revealing that they look very similar. The largest difference is the peak measured by the buoys on 27 September which is not seen in the model. This peak corresponds to the cyclone Gulab which seems not to be in the SWAN model. The wave directions for both datasets can be seen in Figure 5.4. Appendix K.2 shows for the locations KP25, KP7W and KP7E that the significant wave heights and wave directions are very similar. However, in the figure of KP7W and KP7E is again seen that the SWAN model does not show higher values during the cyclone Gulab. It is therefore concluded that this cyclone is not registered in the SWAN model. However, because the SWAN dataset is relatively short, it cannot be concluded that all storms are not captured by the model.

Additionally, the dataset of SWAN can explain the peak value of 39E in figure 3.9 in Section 3.3.2, which was not captured by 39C. Figure 4.6b in Section 4.2.2 shows a time instance for which the wave direction is west of the channel, yet the significant wave height east of the channel is slightly higher than in the channel. This explains the higher value captured at 39E.

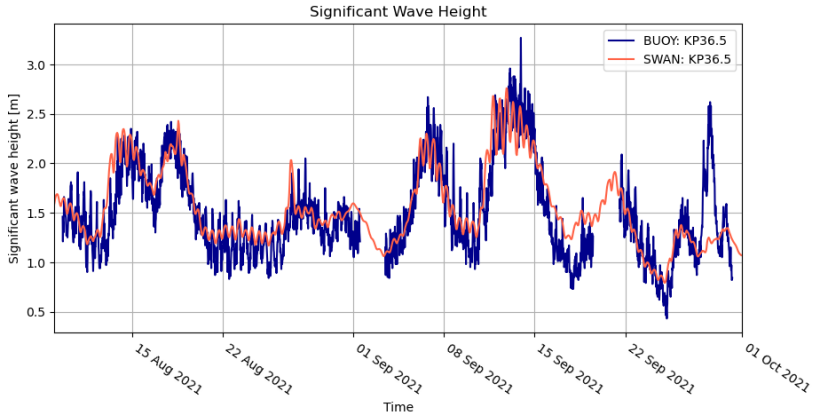

Figure 5.3: Time series of the significant wave height for the buoy data and SWAN data of the location KP36.5 .

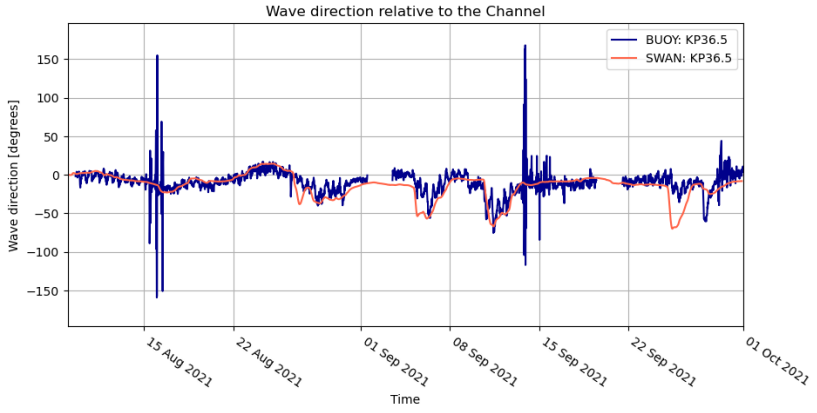

Figure 5.4: Time series of the wave direction for the buoy data and SWAN data of the location KP36.5 .

5.4 Comparison of WW3 model with the SWAN model

The SWAN model can only be compared with the WW3 model at the WW3 point during the SWAN model's time interval. Figure 5.5 shows that the significant wave heights between the two models are minimal. The SWAN model produces slightly higher values, potentially due to

the use of different boundaries in the SWAN model.

The wave directions for both models are shown in Figure 5.6. The direction for both models align closely with the channel orientation, indicating that the wave directions in both models are sufficiently similar to be a good representative of the actual measured wave directions.

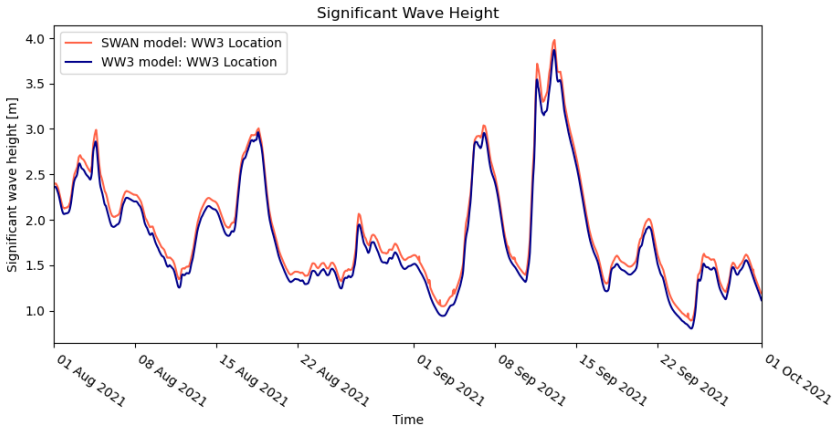

Figure 5.5: Time series of the significant wave height of the SWAN model and WW3 model for the WW3 point.

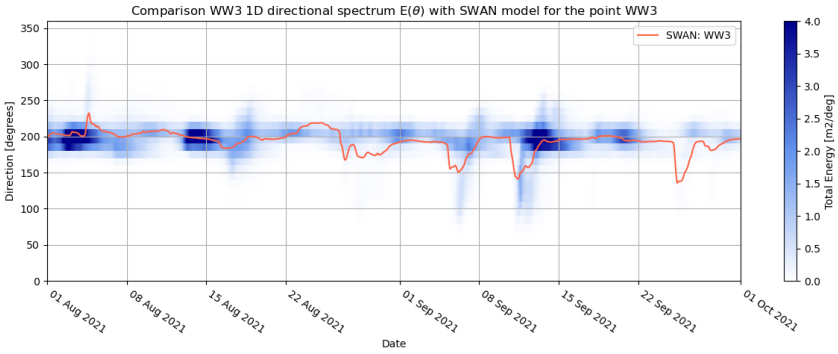

Figure 5.6: Time series of the wave direction of the SWAN model and WW3 model for the WW3 point.

6 Conclusions

The objective of this thesis is to investigate the change in significant wave height and wave direction from offshore to nearshore near the channel in the Bay of Bengal at the coast of Bangladesh using buoy data and the WW3 and SWAN model. First, each sub question is answered to answer the two primary research questions to conclude the findings of this thesis.

Sub question 1: What are the characteristics of the waves based on the measurements of the buoys?

The analysis of buoy data revealed that significant wave heights decrease as they propagate towards the coast, with a significant reduction from KP28E onwards due to increased seabed influence. The data also shows that the significant wave height increases during the monsoon season and when cyclones and depressions occur in the Bay of Bengal. Furthermore, wave directions at the KP locations align closely with the channel orientation, even when the channel orientation changes, due to wave refraction.

Sub question 2: What are the characteristics of the waves based on the WW3 model for offshore and SWAN model for nearshore waves?

The WW3 model showed the significant wave height and wave direction for the 'WW3 point' located farther offshore than KP60. The data showed an increase in significant wave heights during the monsoon season due to stronger winds transferring more energy to the waves. The model captured higher peak values when cyclonic events occurred. The average direction at this point was 198 degrees, aligning well with the channel direction.

The SWAN model results show simulated significant wave heights across the grid, revealing that wave heights decrease as wave approach the coast. The wave heights drop most significantly after KP60, where the water depths decrease significantly. Tidal patterns are visible at most locations, except for WW3 and KP60 where the wave heights are higher. According to the SWAN model, the wave direction remains nearly identical across locations, even when the channel orientation changes.

Sub question 3: What are the differences of wave characteristics between the measured data and the model results?

The comparison of significant wave heights between buoy measurements and the WW3 model shows that values at the WW3 point are generally higher than at the KP locations. The difference in wave heights increases as waves approach the coast, due to refraction, and wave directions at both the WW3 point and KP locations closely align with channel orientations.

In comparing the buoy data with the SWAN model, only one significant difference in wave height is encountered where the SWAN model did not simulate the peak values corresponding from the cyclone Gulab. The limited time interval of the SWAN dataset restricts definite conclusions about if the model simulates the significant wave heights correct during storm events. The SWAN model does not show wave direction change due to refraction, while the buoy data does show wave direction change.

The comparison between the WW3 and SWAN models at the WW3 point show that the wave heights of the models are almost identical, with the SWAN model's significant wave height being slightly higher. This difference could be due to the SWAN model using a different boundary.

The wave direction of both models are very similar.

Primary research question: How do wave characteristics change from offshore to nearshore and with respect to the channel in the Bay of Bengal near the coast of Bangladesh?

Wave characteristics change significantly from offshore to nearshore, with wave heights decreasing as they move closer to the coast due to seabed interactions. Furthermore, the monsoon season, cyclones and depressions additionally impact these characteristics, resulting in higher wave heights. Additionally, the wave directions change according to the channel direction due to wave refraction.

It can be concluded that the wave heights in the channel are lower than outside the channel due to lower water depths in the channel. Additionally, when waves pass over the channel, the wave heights are minimally affected, decreasing only slightly. When the channel orientation changes, the waves refract with the orientation and loose energy resulting in lower wave heights.

7 Recommendations

In this chapter, recommendations are provided to improve the research on the analyzed wave characteristics and the comparison of the datasets.

The two wave characteristics analyzed in this thesis are the significant wave height and the wave direction. Based on the figures, conclusions have been drawn about the correlation between different KP locations. To further substantiate these conclusions, a scatter plot can be created between the locations to visualise the correlation.

To further investigate wave characteristics in the Bay of Bengal, parameters such as wave period or celerity could be examined. These characteristics would help identify wave lengths, wave energy and wave frequencies of the locations. Additionally, the wave tides could be more examined of the buoy measurements and seeing weather the buoys have captured these right.

The dataset of the SWAN model was a very short, covering only 2 months, which is to short to say whether all cyclones are not simulated in the SWAN model. Therefore, another study with longer SWAN datasets can give more insights if the model simulates these storms. Additionally, when the data of the SWAN model is larger, the SWAN and WW3 model comparison can be elaborated to determine if the differences remain minimal a other times as well.

References

Balaguru, K., Taraphdar, S., Leung, L., & Foltz, G. (2014). Increase in the intensity of postmonsoon bay of bengal tropical cyclones. *Geophysical Research Letters*, 3594. Retrieved from https://doi.org/10.1002/2014gl060197

Basco, D. R. (n.d.). *A qualitative description of wave breaking.* Retrieved from https://ascelibrary.org/doi/pdf/10.1061/%28ASCE%290733-950X%281985%29111%3A2%28171%29

Cargo & sea management. (n.d.). Retrieved from https://csmshipping.com/about-us/

CIMSS. (2023). *Indian ocean archive.* Cooperative Institute for Meteorological Satellite Studies. Retrieved from https://tropic.ssec.wisc.edu/storm_archive/indian.html

Davidson-Arnott, R. (2010). *Introduction to coastal processes and geomorphology.* Campridge University Press.

de Nul, J. (n.d.). *Bouw van de zeehaven payra in bangladesh.* Retrieved from https://www.jandenul.com/nl/projecten/bouw-van-de-zeehaven-payra-bangladesh

EPSG. (n.d.). *Transform coordinates.* Retrieved from https://epsg.io/transform#s_srs=37202&t_srs=102955&x=90.0000000&y=21.0000000

Holthuijsen, L. H. (2007). *Waves in oceanic and coastal waters.* Campridge University Press.

Masselink, G., Hughes, M., & Knight, J. (2011). *Introduction to coastal processes & geomorphology.* University of Florida.

Matin, N., K.M. Raju, S., & Ataur Rahman, M. (2020). *Analysis of wave characteristics along the coast of bangladesh using a coupled wave-hydrodynamic delft3d model of the bay of bengal.* IOP Conference Serie. Retrieved from https://iopscience.iop.org/article/10.1088/1755-1315/527/1/012013/pdf

Munk, W. (1949). *The solitary wave theory and its application to surf problems.* New York Academy of Science.

NOAA. (n.d.-a). *Tides.* National Oceanic and Atmospheric Administration. Retrieved from https://www.noaa.gov/jetstream/ocean/tides

NOAA. (n.d.-b). *Wavewatch iii model description.* National Oceanic and Atmospheric Administration. Retrieved from https://polar.ncep.noaa.gov/waves/wavewatch/

NOAA. (2023, September). *Tropical cyclone introduction.* National Oceanic and Atmospheric Administration. Retrieved from https://www.noaa.gov/jetstream/tropical/tropical-cyclone-introduction

NRDC. (2018, September 13). *Bangladesh: a country underwater, a culture on the move.* The Natural Resources Defense Council. Retrieved from https://www.nrdc.org/stories/bangladesh-country-underwater-culture-move

SourceForge. (n.d.). *Features of swan.* Retrieved from https://swanmodel.sourceforge.io/features/features.htm

van der Reijden, I. (2020). *Modelling refraction of waves over tidal channels* (Unpublished master's thesis). TU Delft.

WMO. (2023, May 13). *Very severe cyclonic storm mocha threatens myanmar, bangladesh.* World Meteorological organization. Retrieved from `https://wmo.int/media/news/very-severe-cyclonic-storm-mocha-threatens-myanmar-bangladesh`

WorldAtlas. (n.d.). *Maps of bangladesh.* Retrieved from `https://www.worldatlas.com/maps/bangladesh`

Xu, Y., Chen, H., Zhang, G., Wang, R., & Tao, R. (2021). *Analysis wave characteristics in the southeastern bengal bay based on different data sources.* IOP Conference Serie. Retrieved from `https://iopscience.iop.org/article/10.1088/1755-1315/621/1/012083/pdf`

Appendices

A Literature review

Figures A.1 and A.2 show the seasonal wave roses for the OWI and ECMWF data. From both figures can be concluded that the ECMWF data simulates higher significant wave heights. Additionally, the wave directions are different for both datasets.

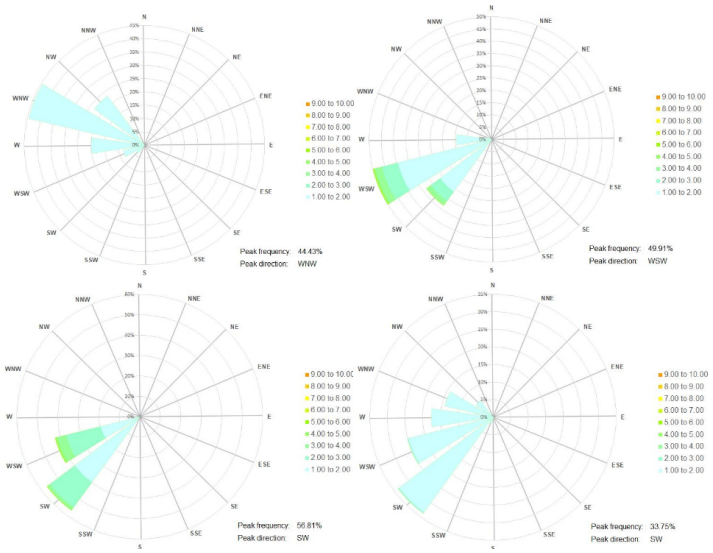

Figure A.1: Seasonal wave rose showing the direction and magnitude of the significant wave height based on OWI data.

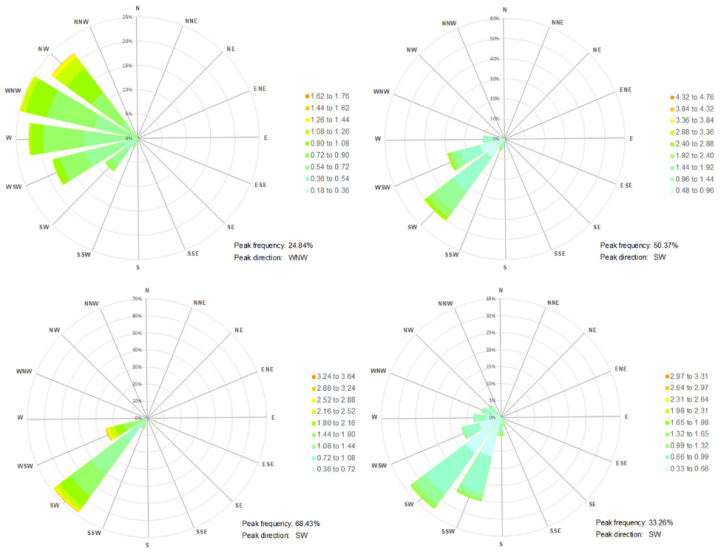

Figure A.2: Seasonal wave rose showing the direction and magnitude of the significant wave height based on ECMWF data.

B The buoy data set

All buoy data captured at the ocean near the coast of Bangladesh has been translated into an Excel file. This Excel file gives wave data for time instances of 30 minutes. The buoys have captured data from May 2021 until July 2023 for the KP locations 60E, 42E, 41E, 39C, 39E, 36.5E, 28E, 26.5E, 25E, 24.5C, 24.5E, 22.5E, 19E, 16C, 16W, 15W, 15E, 7W, 7E, 6W, 6E, -17W and -19.5W.

In the Excel file, the time periods for KP22.5E and KP-19.5W are too short to draw conclusions and are therefore excluded in the analysis. The time periods of the data for 15W and 15E overlap, but their wave characteristics values differ. According to the Excel sheets, both buoys are located at the same coordinates east of the channel. Given the differing values, it is assumed that the coordinates for KP15W are incorrect in the Excel sheet and that the buoy is actually located some distance west of the channel. This assumption allows the data to be included in the analysis.

C Water depths of buoy data

Table 4 shows the water depths for all KP locations for 2021 and 2023. Based on these data the difference in depth between these two years can be calculated for KP locations. The differences highlighted in red are the KP locations for which the water depth has increased or decreased significantly over 2 years.

Table 4: The water depths of all KP locations for which buoys have captured data. The red values indate a signficant increase or decrease in water depth.

KP Location [km]	**2021 [m LAT]**	**2023 [m LAT]**	**recent [m LAT]**	**difference [m LAT]**
60E	-17.52	-	-17.52	0
42E	-7.58	-	-7.58	0
41E	-7.44	-	-7.44	0
39E	-7.26	-	-7.26	0
39C	-7.74	-11.48	-11.48	-3.74
36.5E	-7.46	-	-7.46	0
28E	-6.43	-6.35	-6.35	0.08
26.5E	-6.35	-6.37	-6.37	-0.02
25E	-6.76	-6.77	-6.77	-0.02
24.5E	-6.78	-6.74	-6.74	0.04
24.5C	-6.93	-8.56	-8.56	-1.63
22.5E	-6.92	-6.88	-6.88	0.04
19E	-6.66	-6.83	-6.83	-0.16
16W	-8.04	-8.27	-8.27	-0.23
16C	-8.27	-11.18	-11.18	-2.91
15W	-7.38	-8.31	-8.31	-0.93
15E	-7.01	-8.27	-8.27	-1.26
7W	-7.14	-7.41	-7.41	-0.28
7E	-7.74	-6.45	-6.45	1.29
6W	-6.89	-7.56	-7.56	-0.67
6E	-6.46	-5.73	-5.73	0.73
-17W	-8.79	-8.09	-8.09	0.7
-19.5W	-7.78	-7.69	-7.69	0.09

D Bathymetry

Figure D.1 shows clearly the channel orientation shifts at KP12 and KP-3.

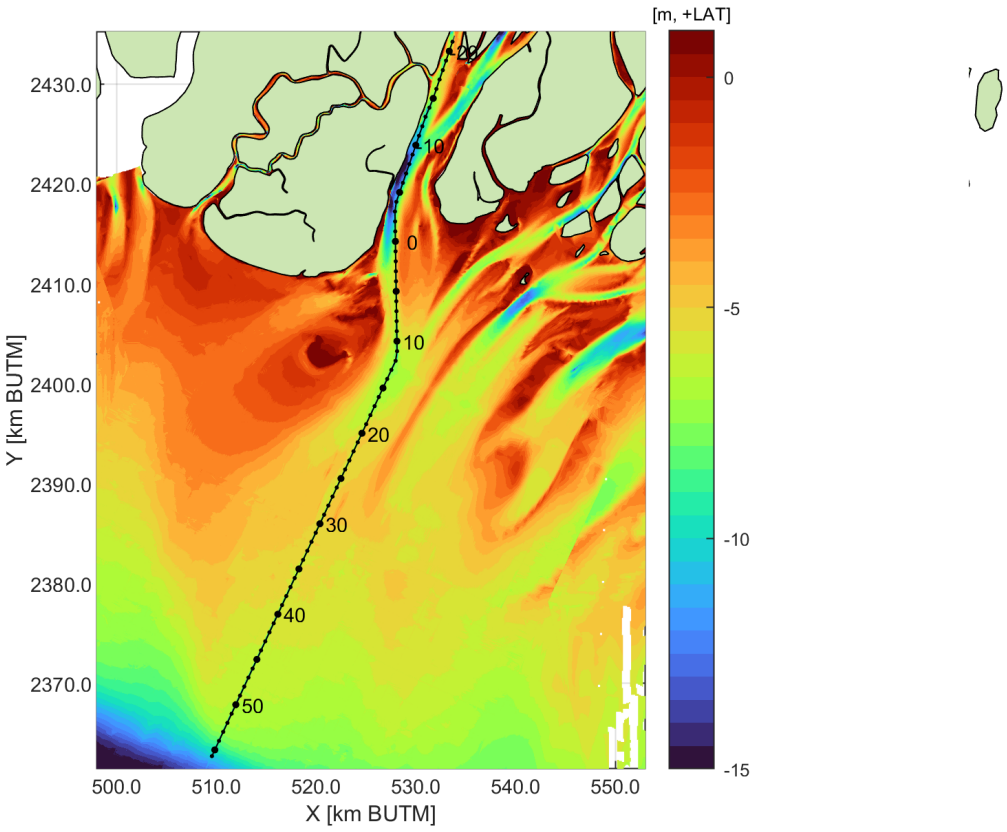

Figure D.1: The bathymetry of the study area zoomed in to clearly see the shifts in channel orientation.

E Significant wave height of KPs far from the coast

Figure E.1 shows that the significant wave height for the KP locations 28, 26.5 and 25 are lower than for the other KP locations. This indicates that after KP36.5 the significant wave height has decreased significantly that can be said that the wave height has decreased.

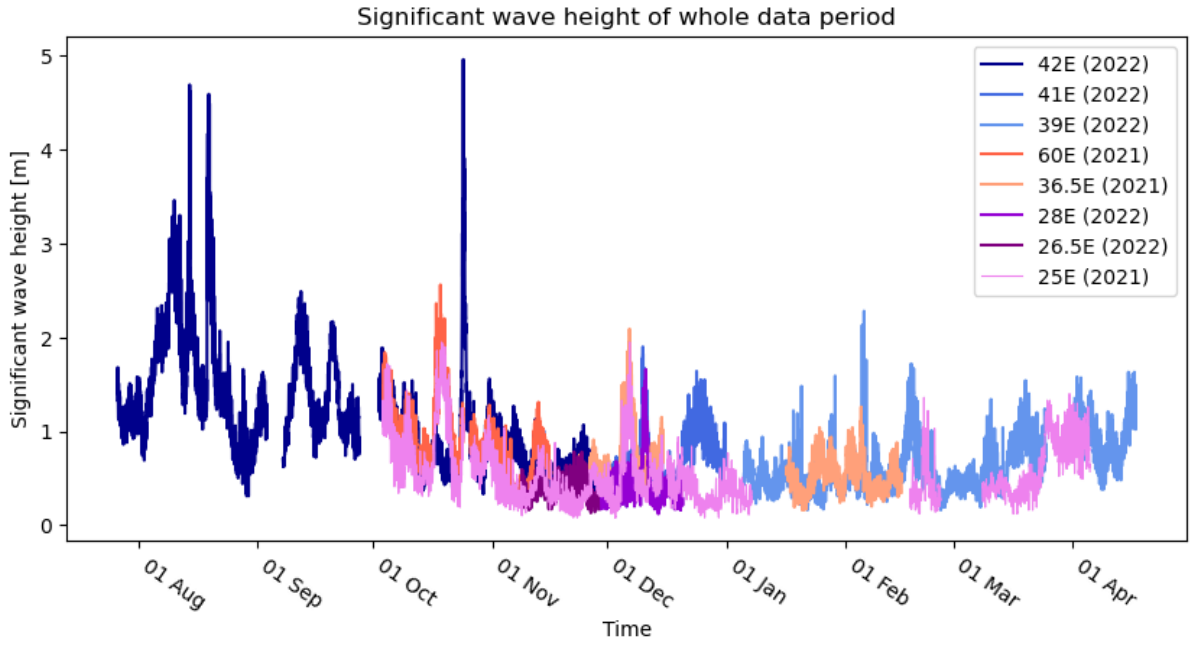

Figure E.1: The significant wave height of KP locations far away from the coast. The time is only expressed in months, not in years showing only data for one year

F Significant wave height per KP

In figures F.2 though F.21, sorted chronologically, the significant wave heights along with the recorded cyclones and depressions are visualised for each KP point.

Cyclones

The first cyclone recorded in the data time frame was the very extreme cyclone Yaas, which was only captured by KP25, as shown in figure F.1. The significant wave height at its peak was slightly over 4 meters. The second cyclone, cyclonic storm Gulab, occurred close to the coast and the locations KP36.5, KP7W and KP7E have data during the time period. While it resulted in peak values, these values were lower than those observed during the first depression. The third cyclonic storm, named Jawad, occurred in December, when overall peak values are lower because it is outside the monsoon period. The peak values were lower than those observed during cyclone Gulab. However, in relative terms to the surrounding values during cyclonic events, the increase in significant wave height was higher of Jawad then Gulab. Cyclone Sitrang, the forth cyclone, has been captured by KP25, KP42 and KP6E. In all three figures F.1, F.6 and F.8 the increase in significant wave height was remarkable. This cyclone originated at the coast of Bangladesh and continued south very close by the channel. Consequently, these KP locations have captured high values, despite the fact that Sitrang is not a severe cyclone during the observed period. The severe cyclonic storm Mandous, the fifth cyclone recorded, occurred south of the coast, near the latitude of south India. The figures F.10, F.11 and F.12 are of KP19E, KP41 and KP28E respectively. The significant wave height patterns in these figures are nearly identical, with an increase near the end date of the storm. This is because the waves formed by the cyclone in the south need time to travel to the coast. The last cyclone captured

is the extremely severe cyclonic storm Mocha captured by KP15E, KP15W and -17.5W. Since the time period of 17.5W, seen in figure F.21, aligns almost exactly with the cyclone's duration, it is hard to determine if these wave heights are high because they cannot be compared. Figures F.19 and F.20 show that the significant wave height of KP15E is higher relatively to KP15W. This is likely because the storms trajectory is east from the channel.

Depressions

The first depression was recorded by KP36.5, 7E and 7W in the figures F.2, F.3 and F.4 respectively. Despite depressions typically corresponding to less severe weather conditions and lower wind speeds compared to cyclones, this particular depression caused relatively high peaks. This occurred because the depression was in the area close to the coast. The second and third depression were also located close to the coast. Figure F.6 of KP42 clearly shows that these depressions caused high significant wave heights. These depressions were also recorded in figures F.1 and 3.4, but in these cases, the wave heights were not significantly higher that wave heights around these time instances. The fourth and fifth depressions occurred far south of the coast, near the latitude of Sri Lanka and the southern tip of India. Consequently, as shown in figures F.11, F.13 and F.14, the depressions did not result in high peak values.

Figures of cyclones and depressions per KP

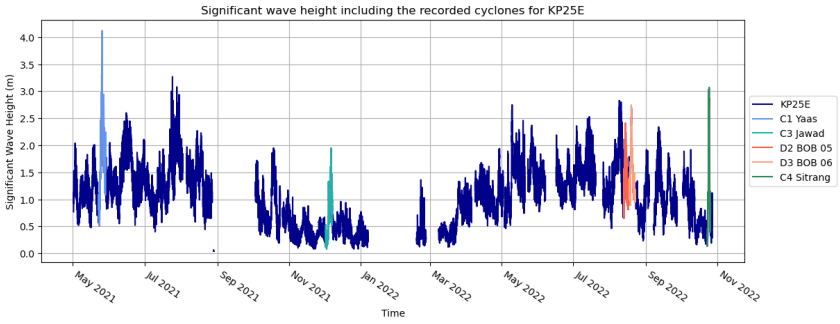

Figure F.1: Time series of the significant wave height of KP25 with all cyclones and depression registered in the time series.

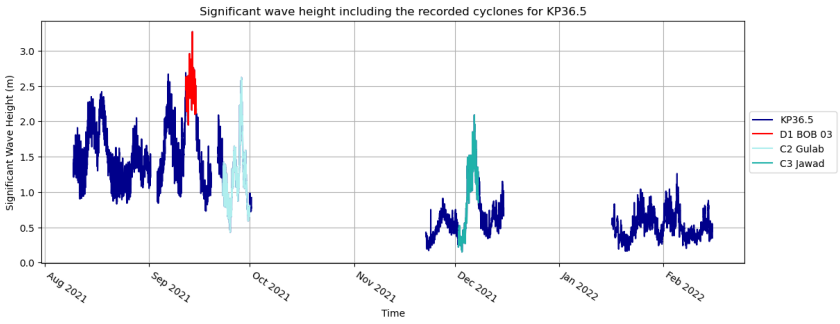

Figure F.2: Time series of the significant wave height of KP36.5 with all cyclones and depression registered in the time series.

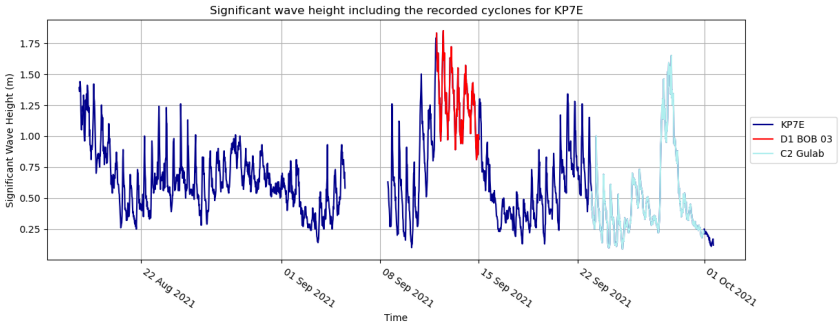

Figure F.3: Time series of the significant wave height of KP7E with all cyclones and depression registered in the time series.

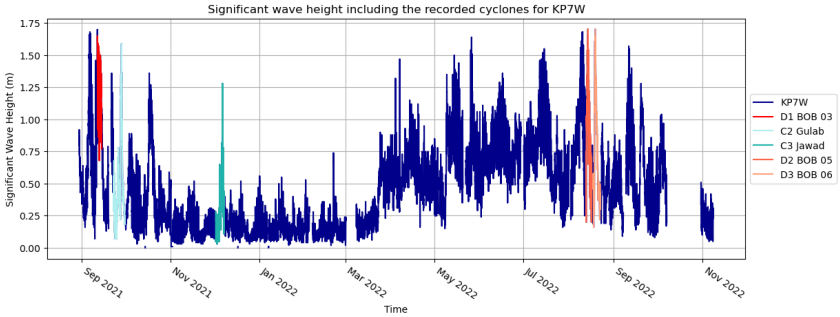

Figure F.4: Time series of the significant wave height of KP7W with all cyclones and depression registered in the time series.

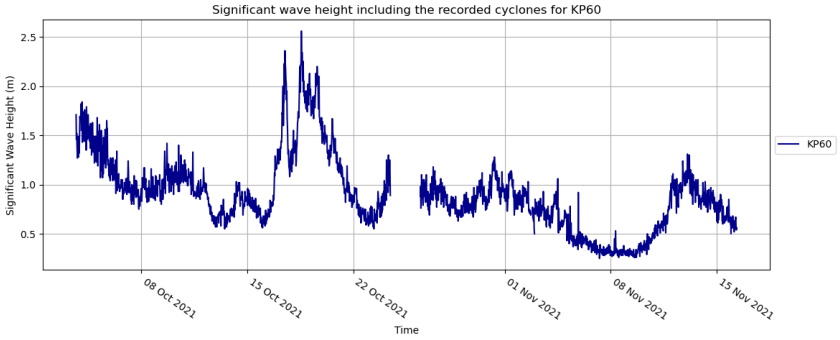

Figure F.5: Time series of the significant wave height of KP60 with all cyclones and depression registered in the time series.

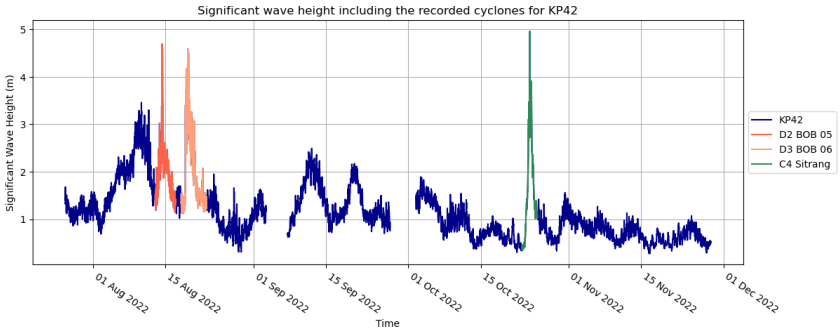

Figure F.6: Time series of the significant wave height of KP42 with all cyclones and depression registered in the time series.

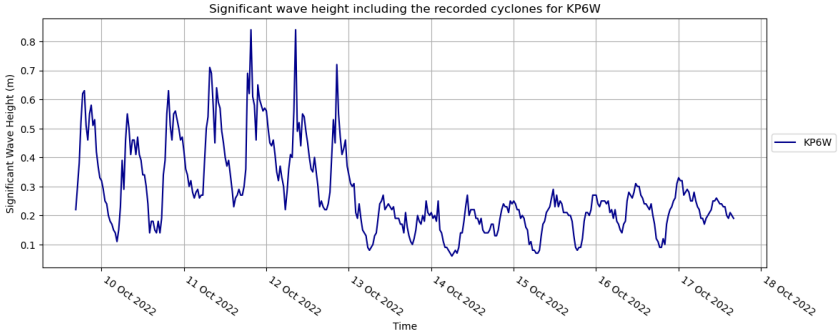

Figure F.7: Time series of the significant wave height of KP6W with all cyclones and depression registered in the time series.

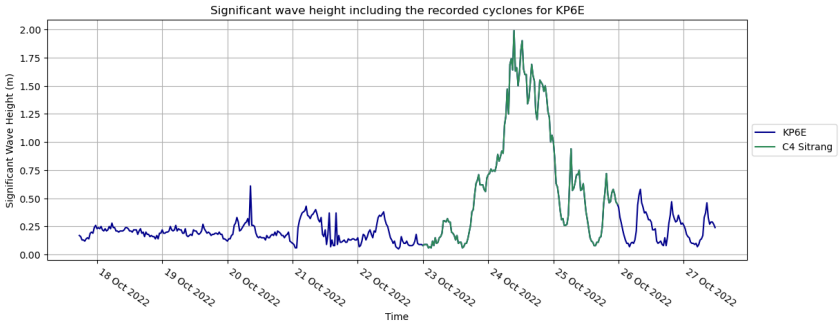

Figure F.8: Time series of the significant wave height of KP6E with all cyclones and depression registered in the time series.

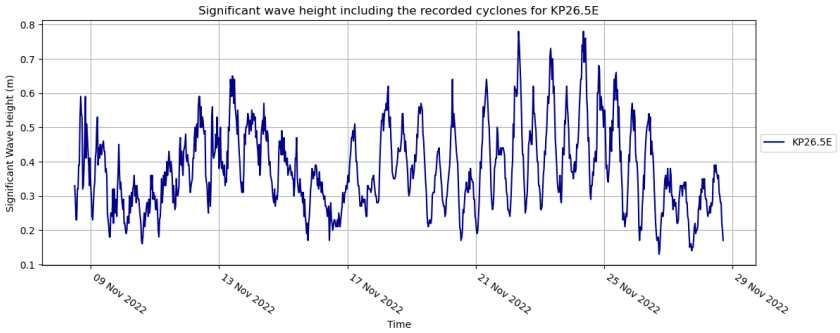

Figure F.9: Time series of the significant wave height of KP26.5E with all cyclones and depression registered in the time series.

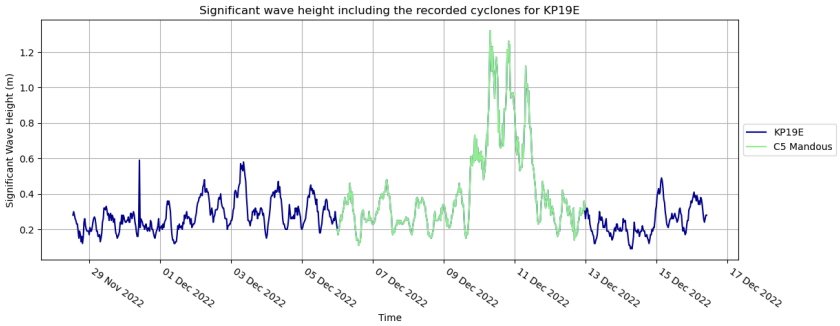

Figure F.10: Time series of the significant wave height of KP19E with all cyclones and depression registered in the time series.

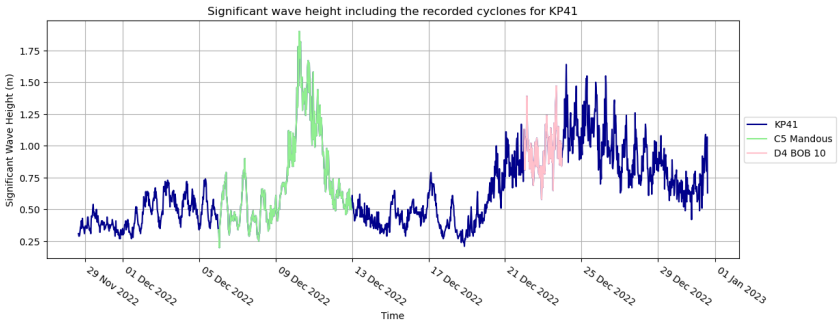

Figure F.11: Time series of the significant wave height of KP41 with all cyclones and depression registered in the time series.

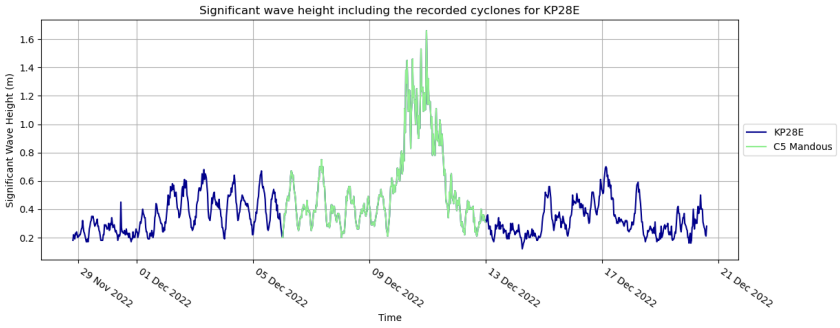

Figure F.12: Time series of the significant wave height of KP28E with all cyclones and depression registered in the time series.

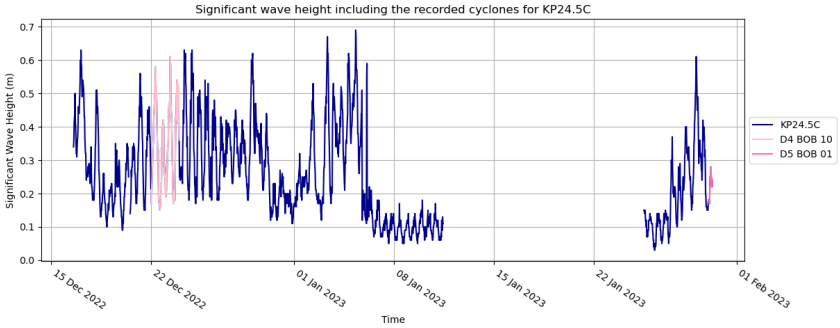

Figure F.13: Time series of the significant wave height of KP24.5C with all cyclones and depression registered in the time series.

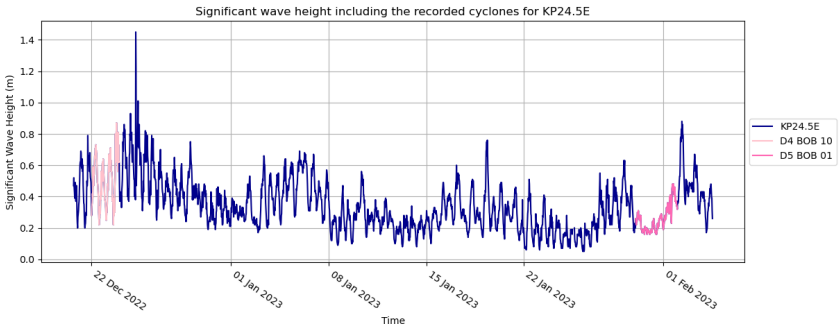

Figure F.14: Time series of the significant wave height of KP24.5E with all cyclones and depression registered in the time series.

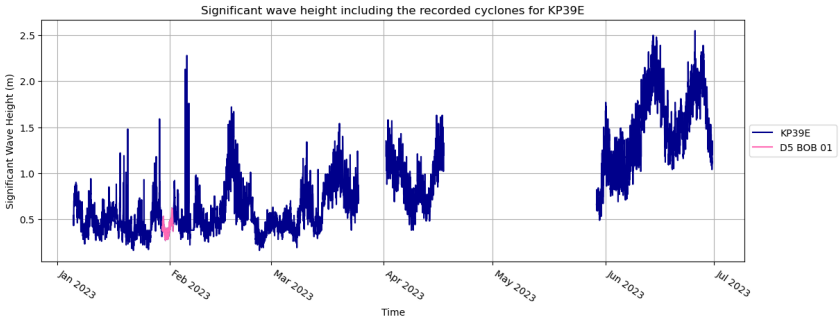

Figure F.15: Time series of the significant wave height of KP39E with all cyclones and depression registered in the time series.

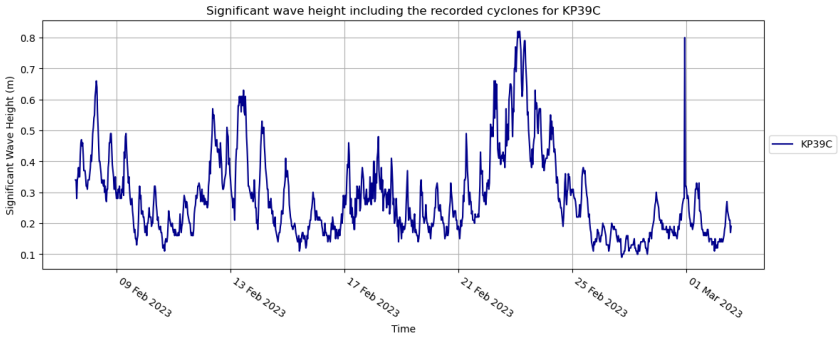

Figure F.16: Time series of the significant wave height of KP39C with all cyclones and depression registered in the time series.

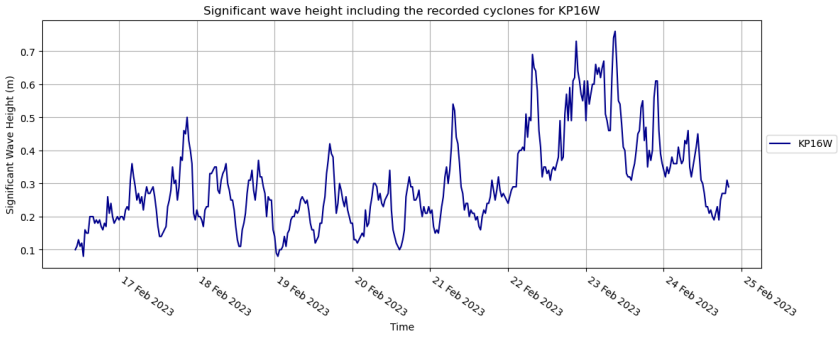

Figure F.17: Time series of the significant wave height of KP16W with all cyclones and depression registered in the time series.

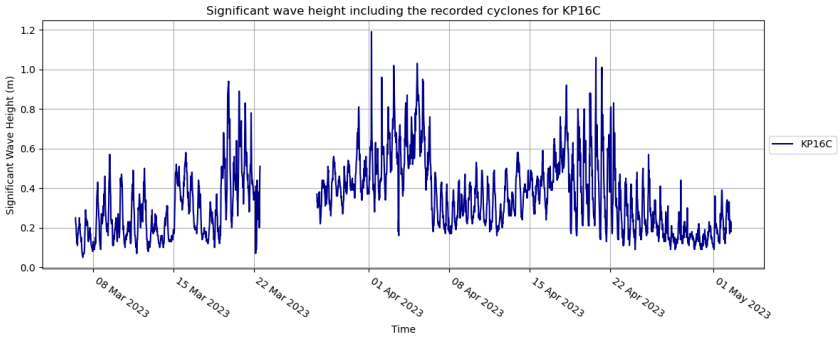

Figure F.18: Time series of the significant wave height of KP16C with all cyclones and depression registered in the time series.

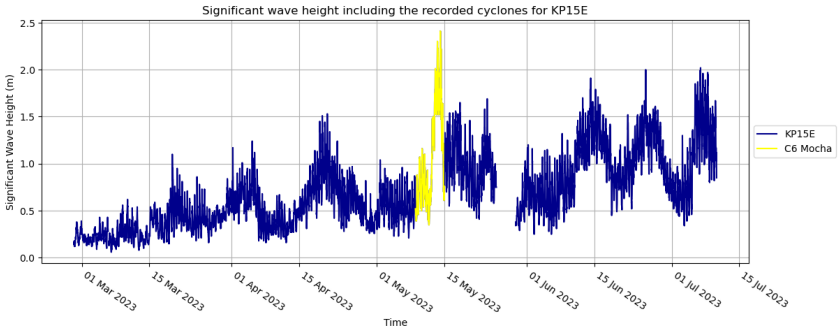

Figure F.19: Time series of the significant wave height of KP15E with all cyclones and depression registered in the time series.

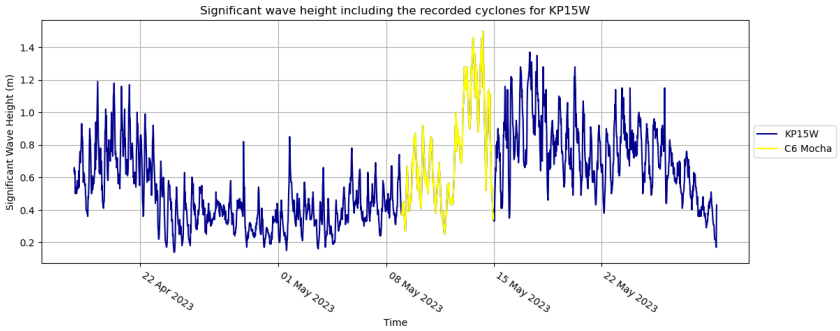

Figure F.20: Time series of the significant wave height of KP15W with all cyclones and depression registered in the time series.

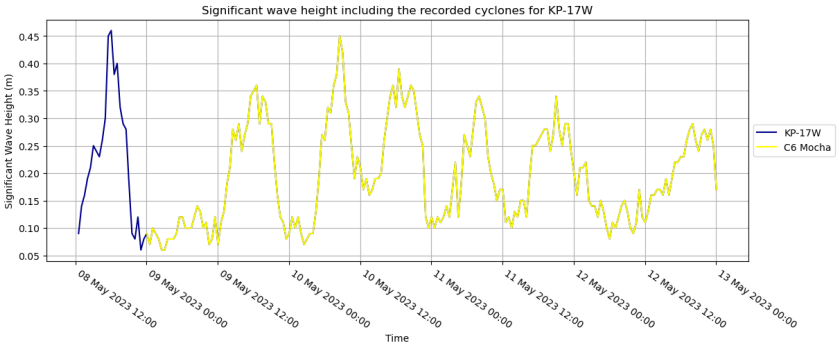

Figure F.21: Time series of the significant wave height of KP-17W with all cyclones and depression registered in the time series.

G Significant wave height comparison

G.1 Comparison between 25 and 7W

In paragraph 3.3.1 the KP locations 25 and 7W were already discussed. In figure G.1 the two long datasets have been combines and this clearly shows that the significant wave height of KP7W is lower compared to KP25.

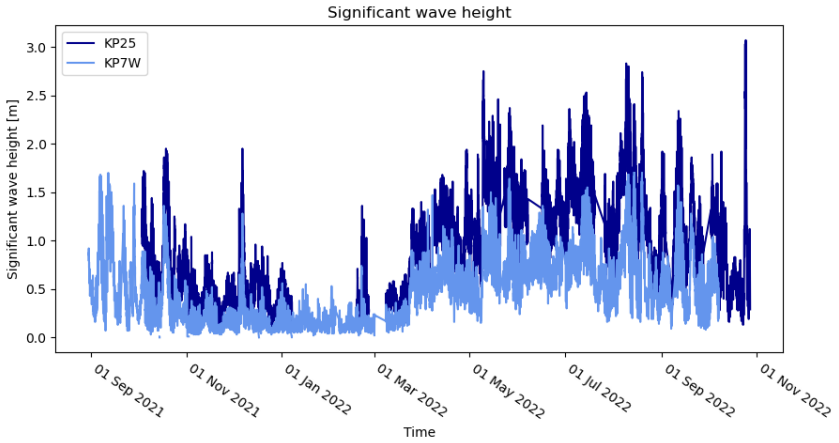

Figure G.1: Time series of the significant wave height of locations 25 and 7W.

G.2 Comparison of KPs with same value

KP24 has data captured at the same time for the channel and east of the channel which can be seen in figure G.2. This figure illustrates that the significant wave height in the channel is lower than at the east, but there is less difference than for KP39. This is possibly because the wave direction is more aligned with the channel than KP39. Additionally, around 4 January and 29 January the significant wave heights are nearly identical. When examining figure G.3, the wave direction generally comes from the west relative to the channel. However, at certain times the wave direction shifts and is coming from the North North East, resulting in lines that span from -170 to 170 degrees. This occurs because the wave direction is plotted within a -180 to 180 degrees range from the channel, causing a small directional change to appear as a large vertical line. These shifts coincide with the times when the significant wave heights are nearly the same. The 180 degree shift in wave direction, can be explained by figure D.1 in appendix D, where can be seen of the bathymetry that water from the delta is being discharged towards the KP from the delta at this angle.

The locations KP7 and KP15 have data on the same time period for the West and East side of the channel. The significant wave height for both locations coincide almost and the wave direction is almost parallel to the channel. For location 7W the 0 degrees is set at an angle of 179.13 degrees because the channel has changed direction after KP12. This indicates that wave refraction has occurred towards the river meeting the ocean at this angle.

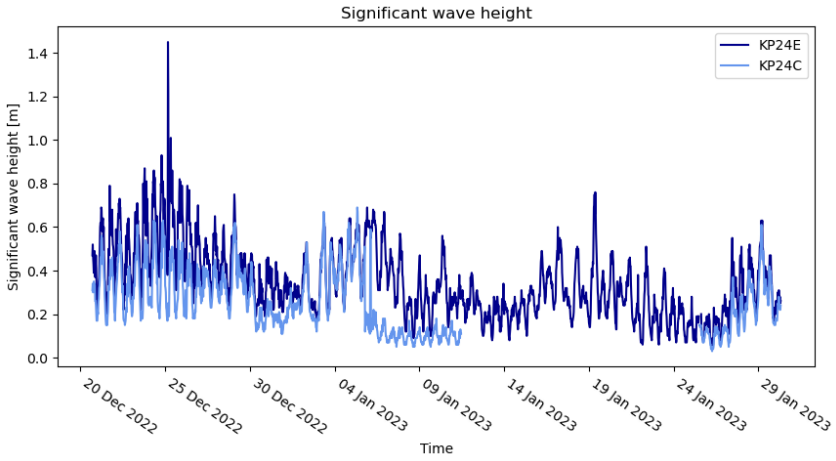

Figure G.2: Time series of the significant wave height of overlap period D comparing KP24E with KP24C.

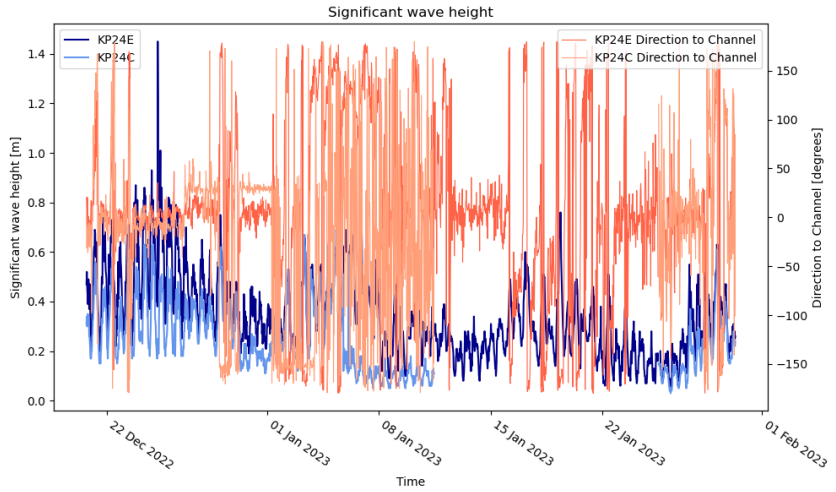

Figure G.3: Time series of the wave direction of overlap period D comparing KP24E with KP24C.

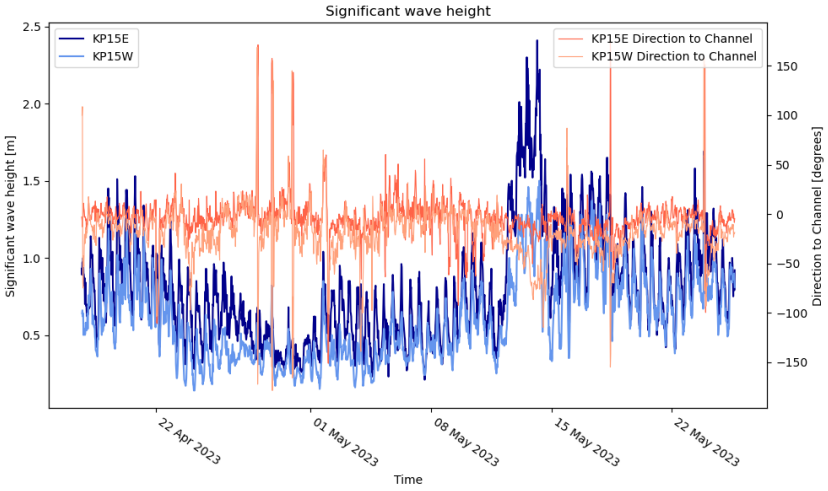

Figure G.4: Time series of the significant wave height of overlap period E comparing KP15E with KP15W.

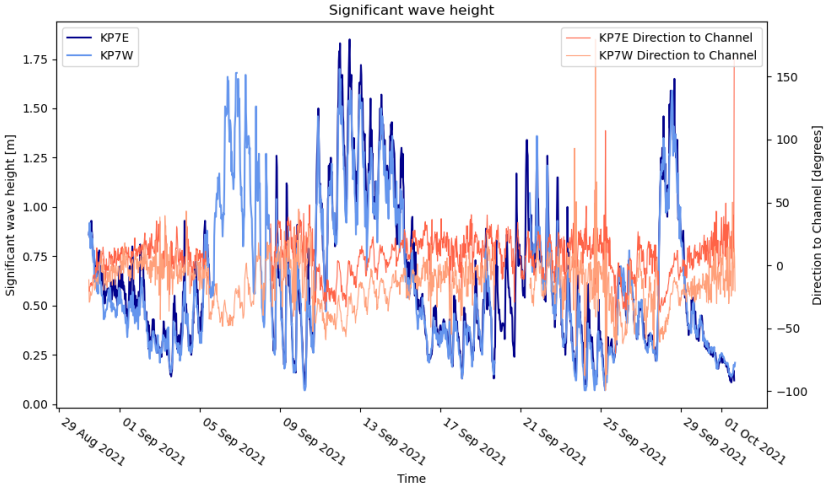

Figure G.5: Time series of the wave direction of overlap period E comparing KP15E with KP15W.

H Wave direction

In figures H.1 though H.21, the significant wave heights, including the wave direction, are shown on the left side, and the wind rose of the corresponding KP location is displayed on the right side. In both figures, the channel direction is indicated by a red line. At all locations, the wave directions fluctuate around the channel. After KP12 the channel rotates from 204.94 to 179.13 degrees. The KP locations 7 and 6 also show wave directions fluctuating along the channel. Therefore, the wave direction has changed by 25 degrees due to wave refraction.

At many locations, the wave direction fluctuates from above 170 degrees to below -170 degrees. As explained in Appendix G.2, this occurs because water from the delta flows in this direction. When a significant amount of water is discharged from the rivers upstream into the sea and there are no extreme weather conditions at the sea, the wave direction reverses, coming from the coast towards the sea.

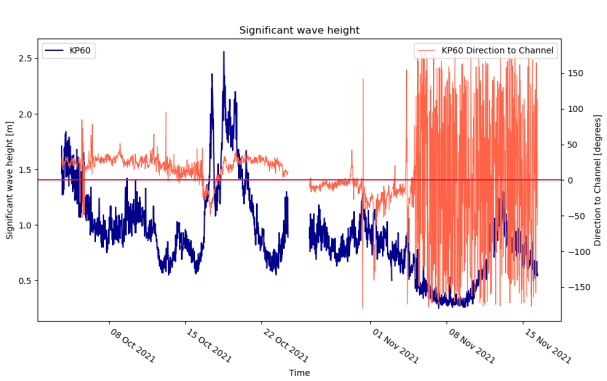

(a) Significant wave height including wave direction

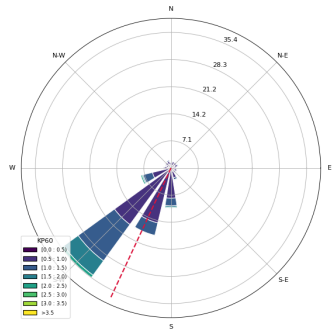

(b) Wave rose including channel direction

Figure H.1: Wave direction of KP60

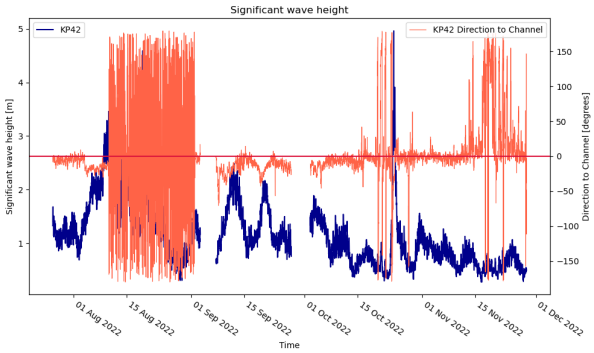

(a) Significant wave height including wave direction

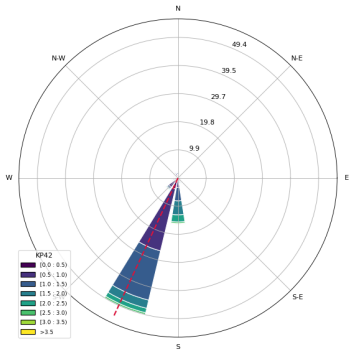

(b) Wave rose including channel direction

Figure H.2: Wave direction of KP42

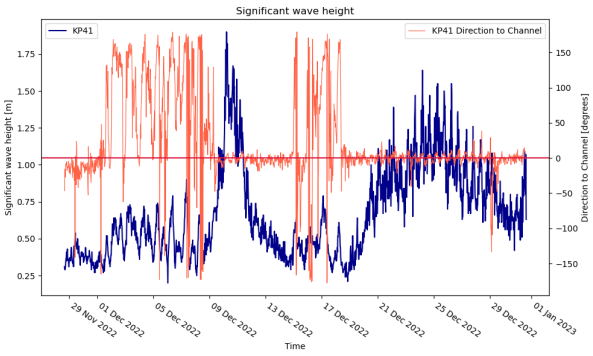

(a) Significant wave height including wave direction

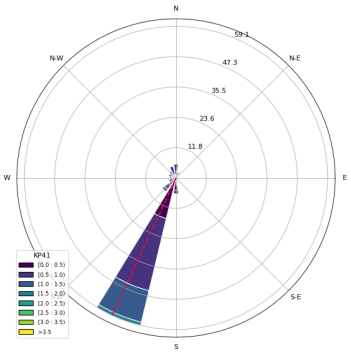

(b) Wave rose including channel direction

Figure H.3: Wave direction of KP41

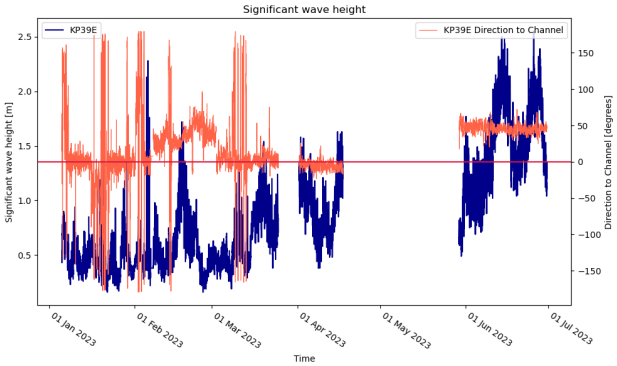

(a) Significant wave height including wave direction

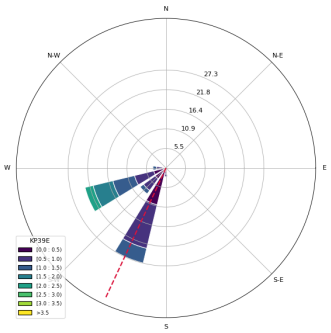

(b) Wave rose including channel direction

Figure H.4: Wave direction of KP39E

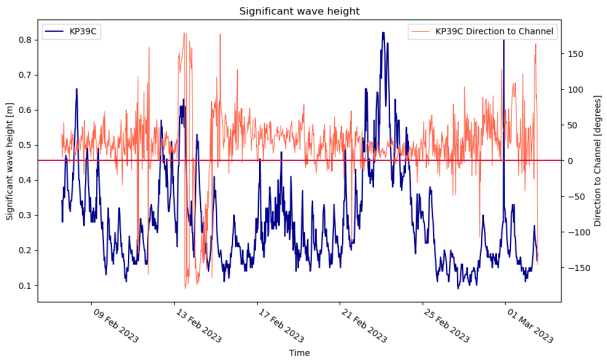

(a) Significant wave height including wave direction

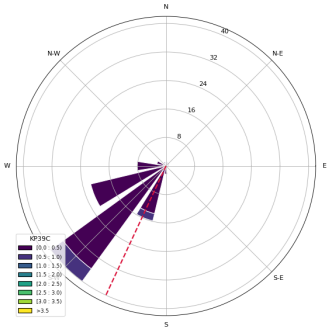

(b) Wave rose including channel direction

Figure H.5: Wave direction of KP39C

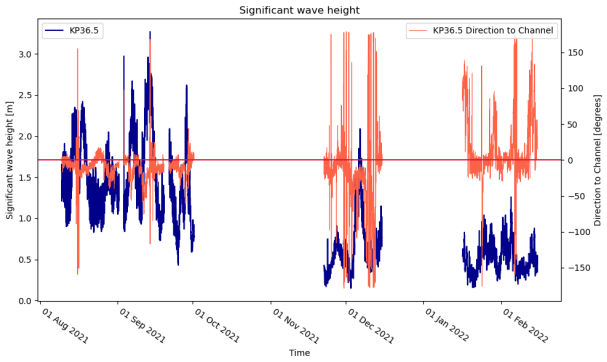

(a) Significant wave height including wave direction

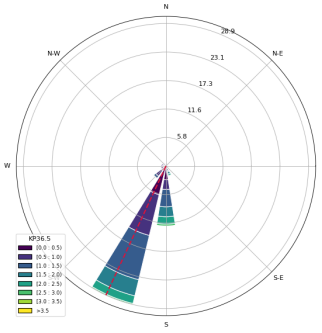

(b) Wave rose including channel direction

Figure H.6: Wave direction of KP36.5

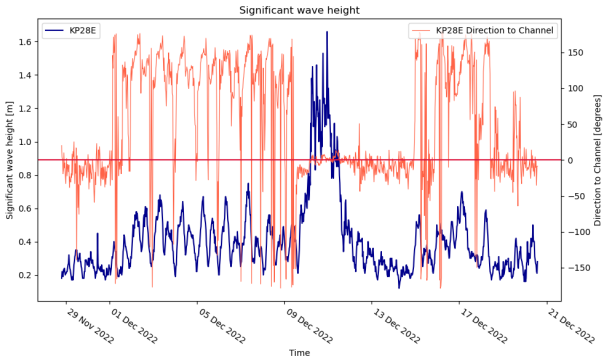

(a) Significant wave height including wave direction

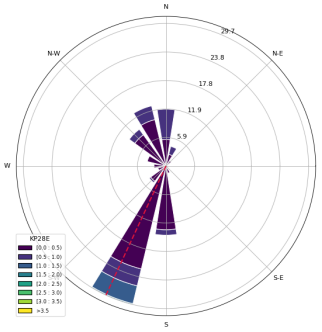

(b) Wave rose including channel direction

Figure H.7: Wave direction of KP28E

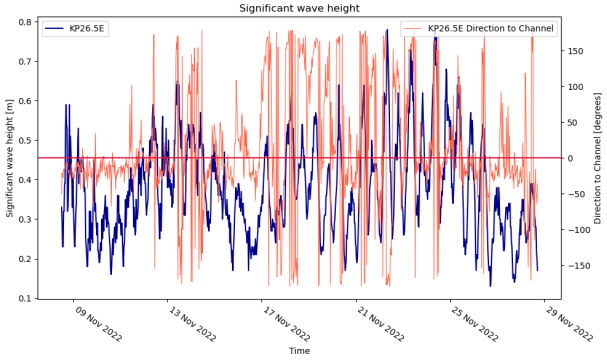

(a) Significant wave height including wave direction

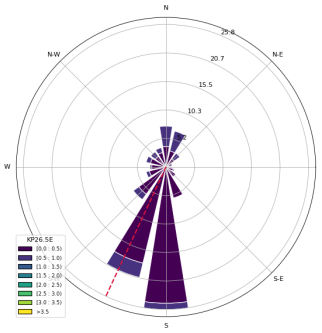

(b) Wave rose including channel direction

Figure H.8: Wave direction of KP26.5E

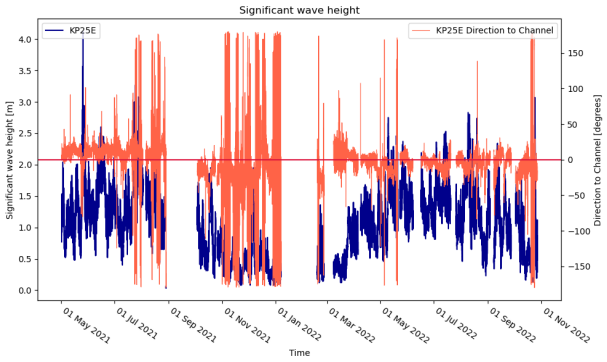

(a) Significant wave height including wave direction

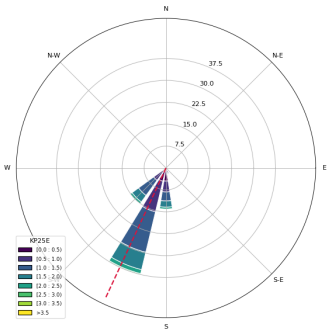

(b) Wave rose including channel direction

Figure H.9: Wave direction of KP25E

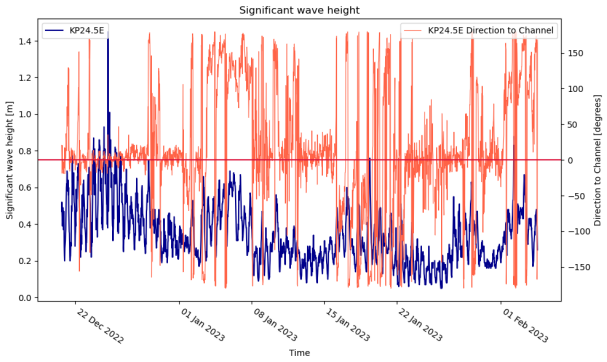

(a) Significant wave height including wave direction

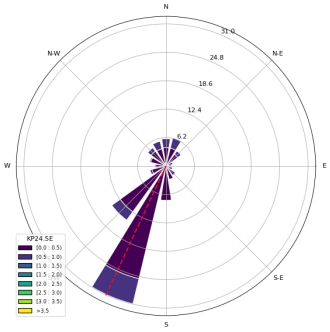

(b) Wave rose including channel direction

Figure H.10: Wave direction of KP24.5E

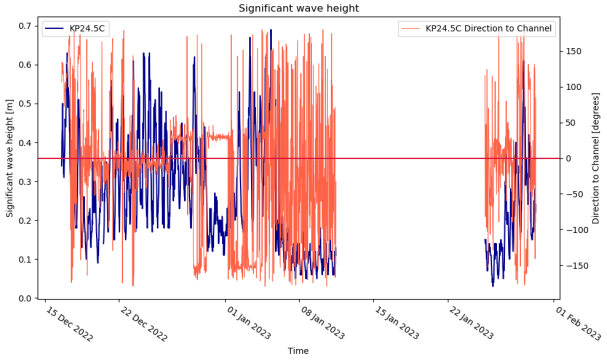

(a) Significant wave height including wave direction

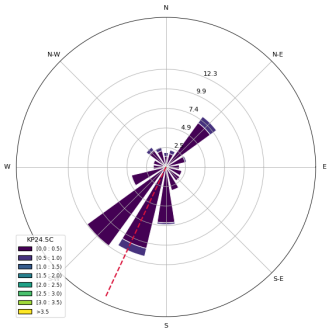

(b) Wave rose including channel direction

Figure H.11: Wave direction of KP24.5C

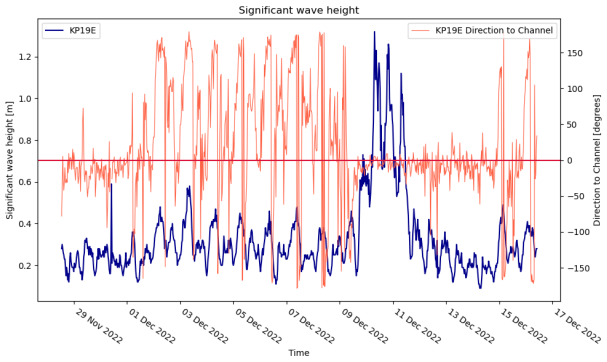

(a) Significant wave height including wave direction

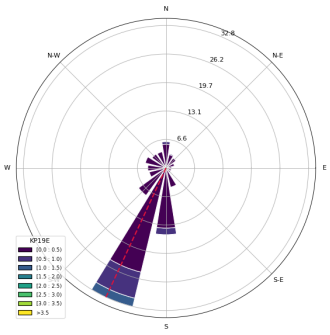

(b) Wave rose including channel direction

Figure H.12: Wave direction of KP19E

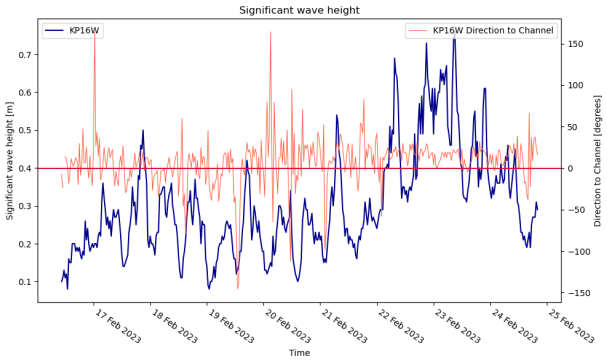

(a) Significant wave height including wave direction

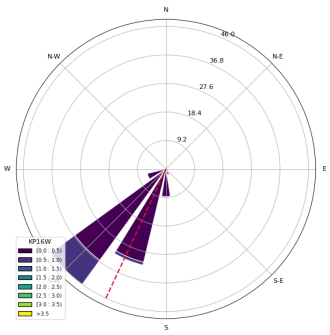

(b) Wave rose including channel direction

Figure H.13: Wave direction of KP16W

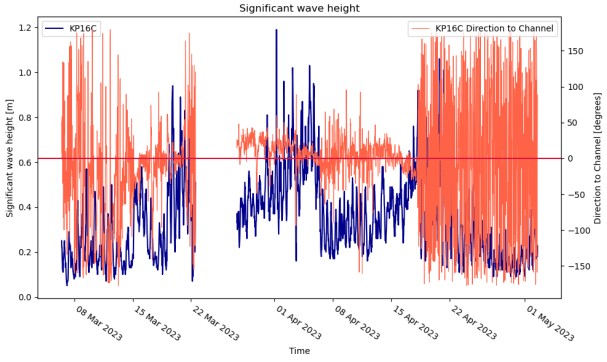

(a) Significant wave height including wave direction

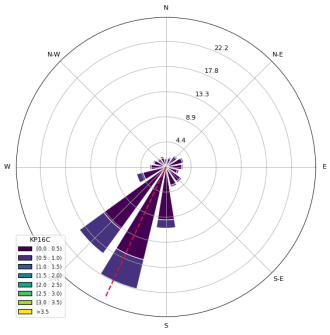

(b) Wave rose including channel direction

Figure H.14: Wave direction of KP16C

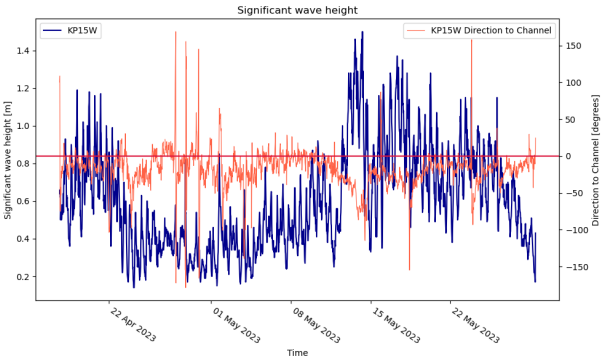

(a) Significant wave height including wave direction

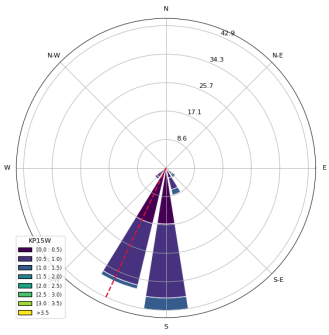

(b) Wave rose including channel direction

Figure H.15: Wave direction of KP15W

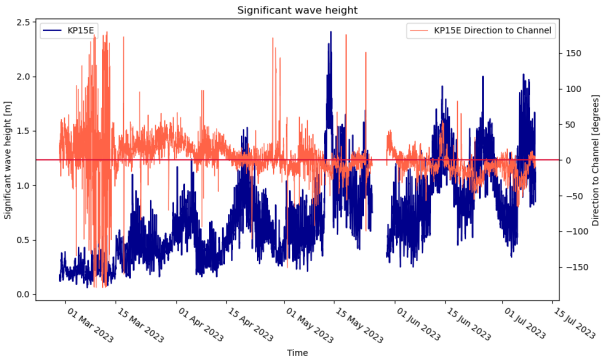

(a) Significant wave height including wave direction

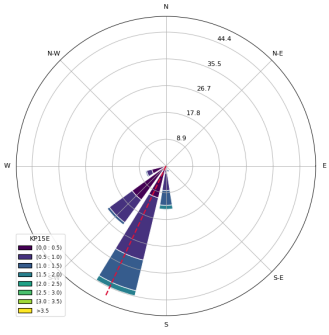

(b) Wave rose including channel direction

Figure H.16: Wave direction of KP15E

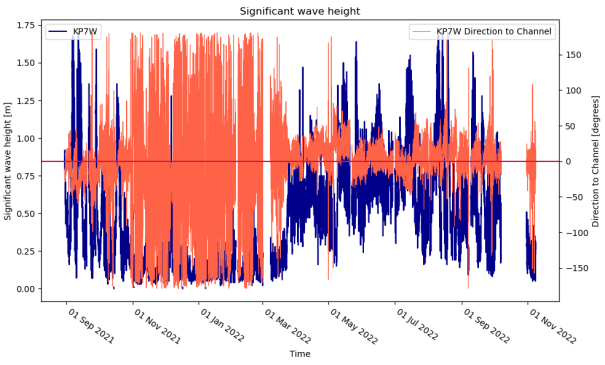

(a) Significant wave height including wave direction

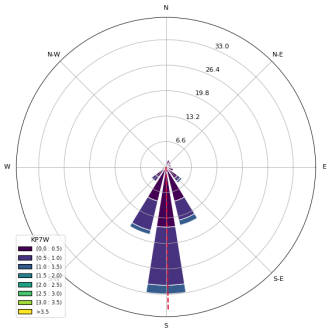

(b) Wave rose including channel direction

Figure H.17: Wave direction of KP7W

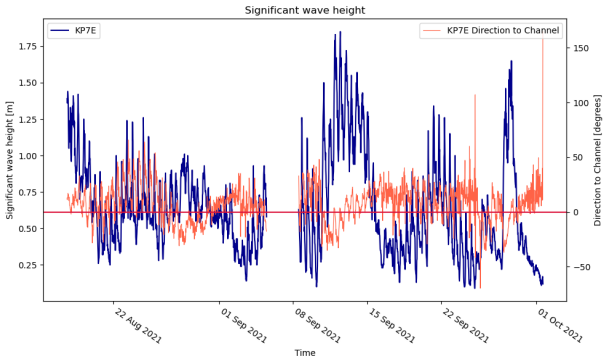

(a) Significant wave height including wave direction

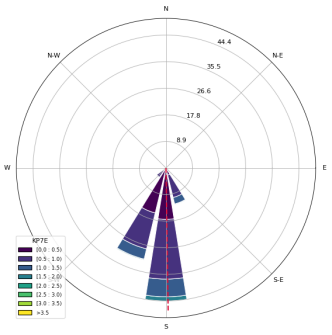

(b) Wave rose including channel direction

Figure H.18: Wave direction of KP7E

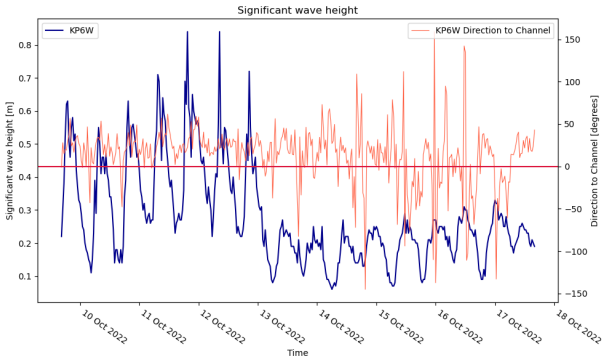

(a) Significant wave height including wave direction

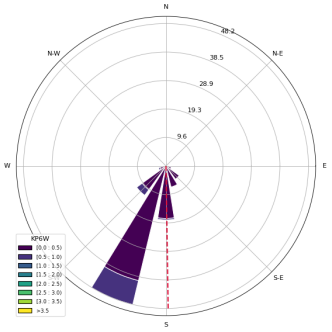

(b) Wave rose including channel direction

Figure H.19: Wave direction of KP6W

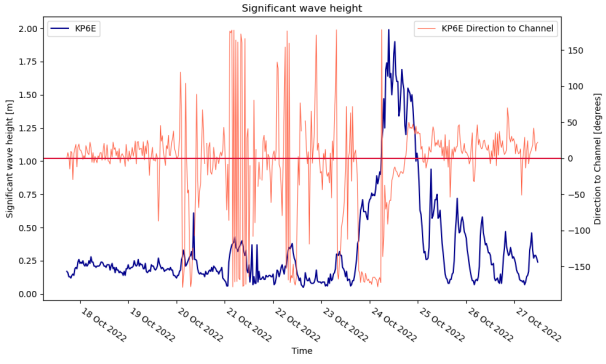

(a) Significant wave height including wave direction

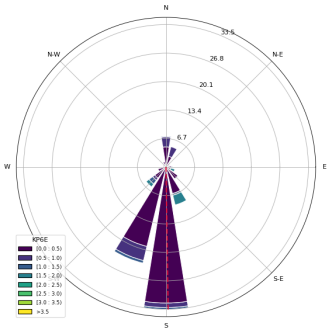

(b) Wave rose including channel direction

Figure H.20: Wave direction of KP6E

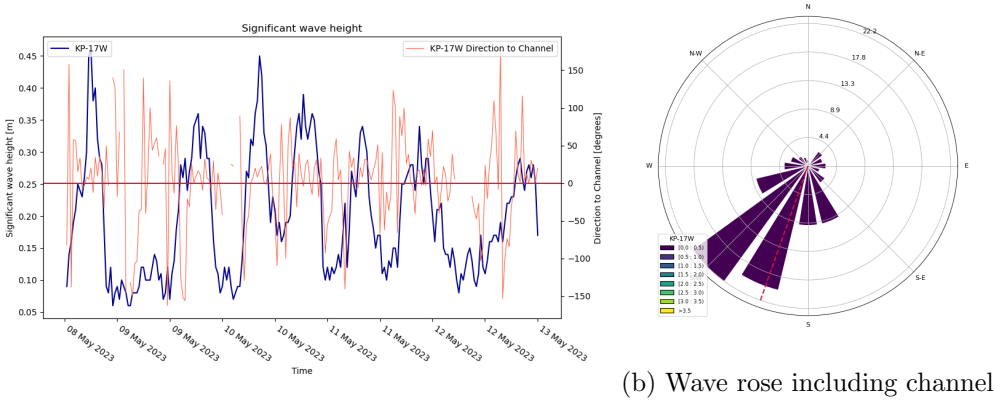

(a) Significant wave height including wave direction

(b) Wave rose including channel direction

Figure H.21: Wave direction of KP-17W

I Results of the WW3 model

Figure I.1 shows the 1D frequency spectrum for the WW3 location across the entire dataset. The frequencies in the Bay of Bengal range from approximately 0.05 Hz and 0.32 Hz, corresponding to swell and wind waves. During the monsoon season, the frequencies are widely distributed, with both swell and wind waves present, and the total energy is higher in the monsoon compared to other months. In the non-monsoon months, the sea primarily consists of swell waves.

Figure I.2 shows the 1D directional spectrum for the WW3 location. The wave direction remains relatively constant over the years, with a slight deviation from the average direction of 200.69 degrees (South-southwest) during the summer. Similar to the frequency spectrum, the total energy is higher during the monsoon season compared to other months. The dotted red line indicates the channel orientation, which is slightly more westward.

Figure I.3 displays the significant wave height derived from the frequency spectrum. In this figure it is also shown that in the monsoon the significant wave heights are significantly higher than in the other months. The highest peak, reaching 11 meters, comes from the super cyclonic storm Amphan, which occurred on May 20, 2020. The peak from 2021 corresponds to the severe cyclonic storm Yaas which was also captured by a buoy as discussed in Chapter 3, with a peak value of 8 meters. The figure also shows that during each monsoon season, the average significant wave height ranges from approximately 2 to 4 meters.

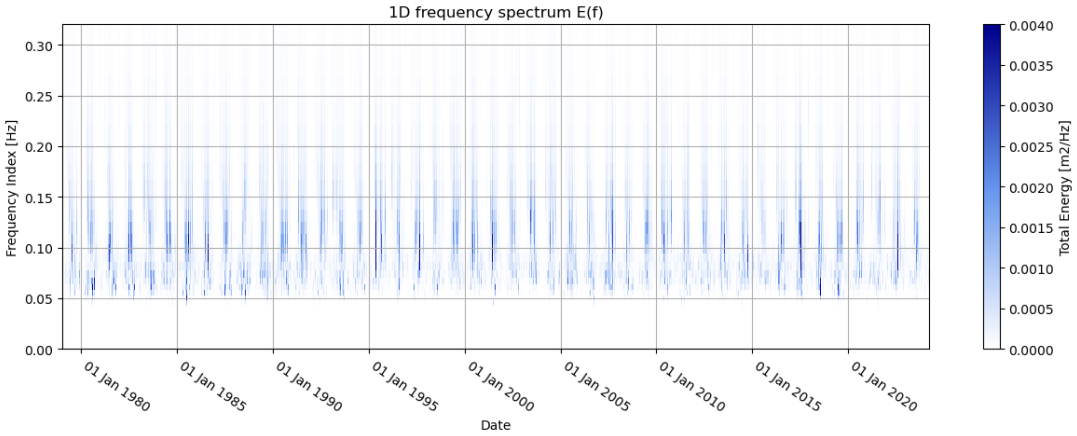

Figure I.1: The 1D frequency spectrum $E(f)$ over the entire time period.

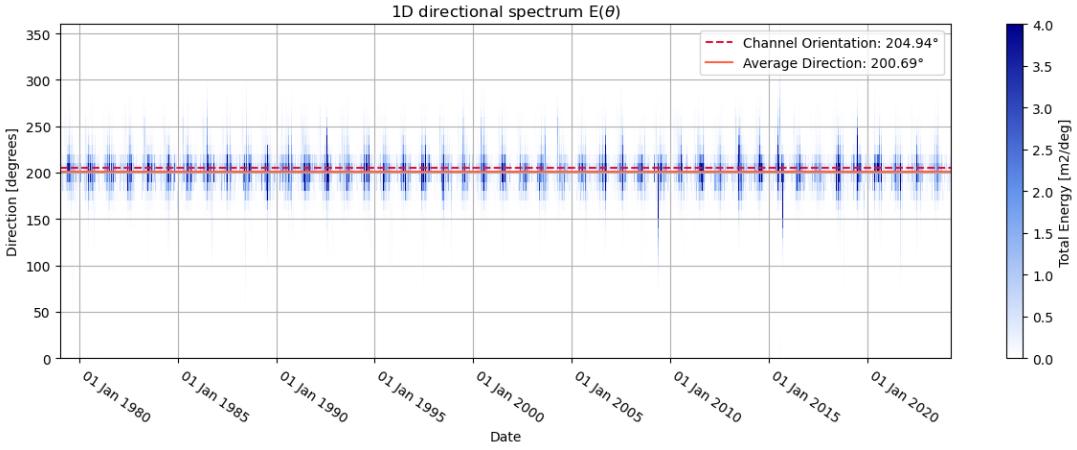

Figure I.2: The 1D direction spectrum $E(\theta)$ over the entire time period.

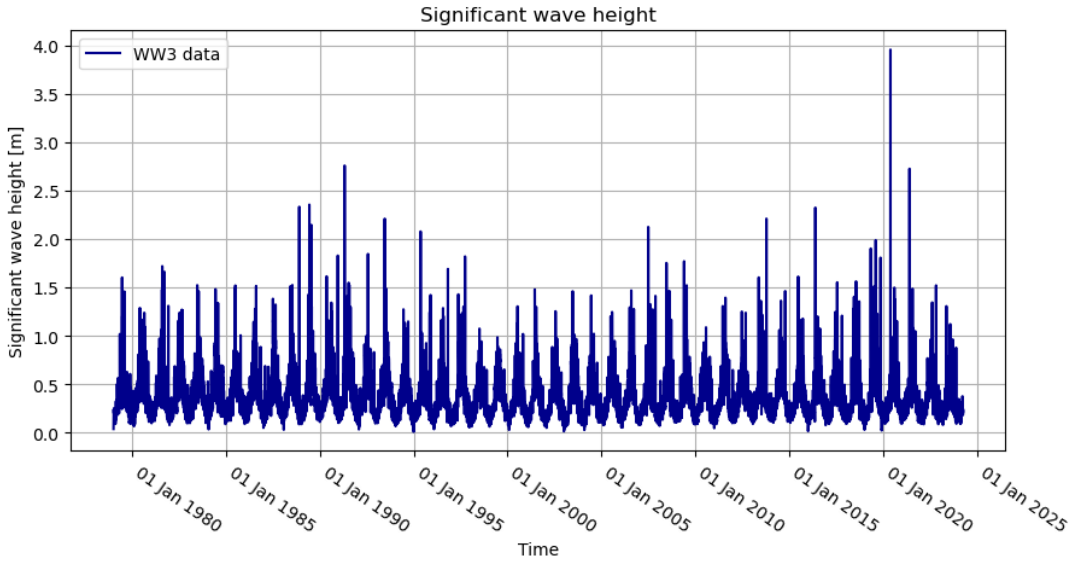

Figure I.3: The significant wave height H_{m_0} over the entire time period.

J The h/L_0 condition

The h/L_0 condition determines whether the water at a given depth can be classified as deep water, where waves are not influenced by the seabed, intermediate water depths or shallow water. The water depth h in the condition is based on the mean sea level (MSL), and the deep water wave length L_0 can be obtained using Equation 12. The deep water wave length is derived from either the wave period or frequency in deep water. In this study, the location of the WW3 point, which is the furthest from the coast, is used to identify whether this point qualifies as deep water.

In the ocean, wave periods and frequencies vary significantly, making it inappropriate to use an average frequency for the entire dataset of the location. Therefore, an average wind wave frequency has been taken and an average swell wave. Additionally, the lowest frequency occurring has been taken as a third point. The selected frequencies are 0.1583 Hz, 0.0787 Hz and 0.054 Hz respectively.

The h/L_0 values that define whether a location is considered deep, intermediate or shallow are discussed in Chapter 2.2.2. Initially, the water depth classification is determined for the WW3 point using the three frequencies and can be seen in Table 5. The table shows that the point qualifies as deep water for wind waves, but not for swell waves. However, as this point is the furthest location from the coast with available data, it is considered as deep water to classify the water type at the KP locations. The result of this can also be seen in Table 5. It can be concluded based on this table, that under swell conditions, all KP points are characterized as shallow, except for KP60. When wind waves are also present, the water depths may transition ti intermediate if wind waves become dominate. It can be concluded that waves are influenced by the seabed from the KP60 onwards, with a significant decrease in water depth from KP60 to KP42 suggesting that beyond KP42 the waves are more affected by the seabed.

$$L_0 = \frac{gT^2}{2\pi} = \frac{g}{f^2 2\pi} \tag{12}$$

Table 5: The h/L_0 condition for deep, intermediate and shallow water types.

KP	Water depth	Number			Type		
	[MSL]	Wind	Swell	Low	Wind	Swell	Low
WW3	69.000	1.107	0.274	0.129	deep	interm	interm
KP60	19.198	0.308	0.076	0.036	interm	interm	shallow
KP42	9.260	0.149	0.037	0.017	interm	shallow	shallow
KP41	9.115	0.146	0.036	0.017	interm	shallow	shallow
KP39E	8.940	0.143	0.035	0.017	interm	shallow	shallow
KP39C	13.158	0.211	0.052	0.025	interm	interm	shallow
KP36.5	9.143	0.147	0.036	0.017	interm	shallow	shallow
KP28E	8.030	0.129	0.032	0.015	interm	shallow	shallow
KP26.5E	8.051	0.129	0.032	0.015	interm	shallow	shallow
KP25	8.454	0.136	0.034	0.016	interm	shallow	shallow
KP24.5E	8.416	0.135	0.033	0.016	interm	shallow	shallow
KP24.5C	10.243	0.164	0.041	0.019	interm	shallow	shallow
KP22.5E	8.555	0.137	0.034	0.016	interm	shallow	shallow
KP19E	8.506	0.137	0.034	0.016	interm	shallow	shallow
KP16W	9.947	0.160	0.039	0.019	interm	shallow	shallow
KP16C	12.856	0.206	0.051	0.024	interm	interm	shallow
KP15W	9.989	0.160	0.040	0.019	interm	shallow	shallow
KP15E	9.953	0.160	0.040	0.019	interm	shallow	shallow
KP7W	9.093	0.146	0.036	0.017	interm	shallow	shallow
KP7E	8.128	0.130	0.032	0.015	interm	shallow	shallow
KP6W	9.236	0.148	0.037	0.017	interm	shallow	shallow
KP6E	7.411	0.119	0.029	0.014	interm	shallow	shallow
KP-17W	9.766	0.157	0.039	0.018	interm	shallow	shallow
KP-19.5W	9.372	0.150	0.037	0.018	interm	shallow	shallow

K Comparison of datasets

K.1 Comparison of buoy measurements and WW3 model

Figures K.1 and 3.7 compare the WW3 point with KP60, KP42, KP25 and KP7W. The data shows that the wave height at WW3 is similar to that at KP60 and the significant wave height is sometimes slightly higher and other times slightly lower. The Figures K.3, K.4, K.5, K.6, K.7, K.8 and K.9 show that the difference between the significant wave height between the KP locations and the WW3 point become larger as the waves propagate towards the coast. Additionally, when peak values are recorded from the buoys, the WW3 point also shows higher significant wave heights.

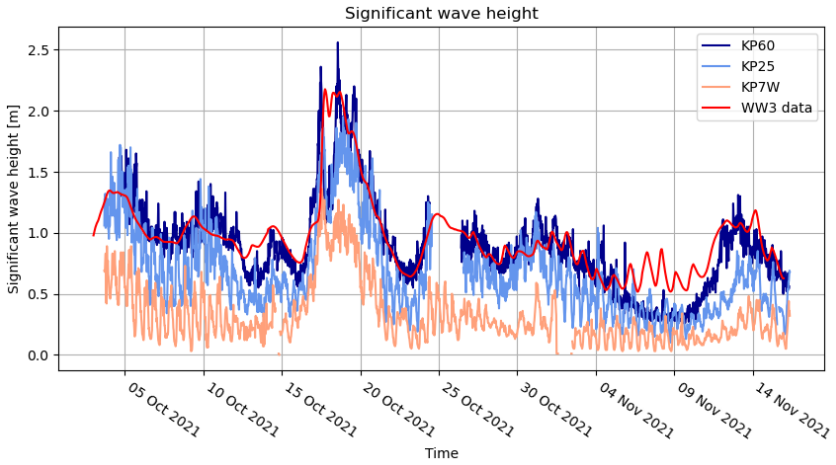

Figure K.1: The significant wave height of the WW3 point of overlap period A of the locations KP60, KP42 and KP7W

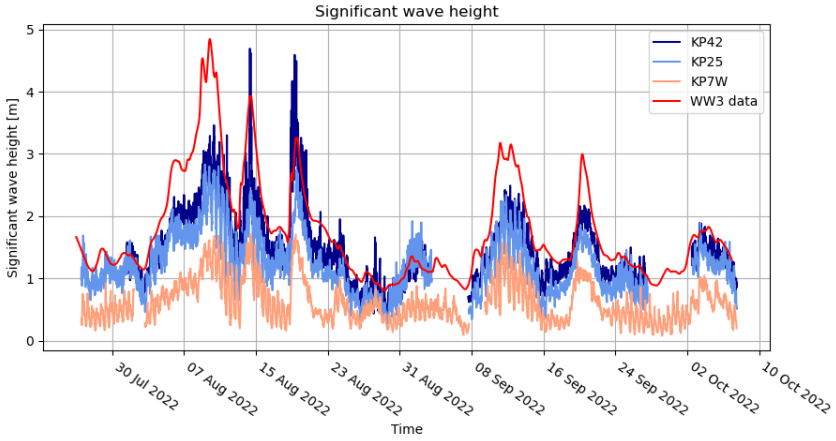

Figure K.2: The significant wave height of the WW3 point of overlap period B of the locations KP42, KP25 and KP7W

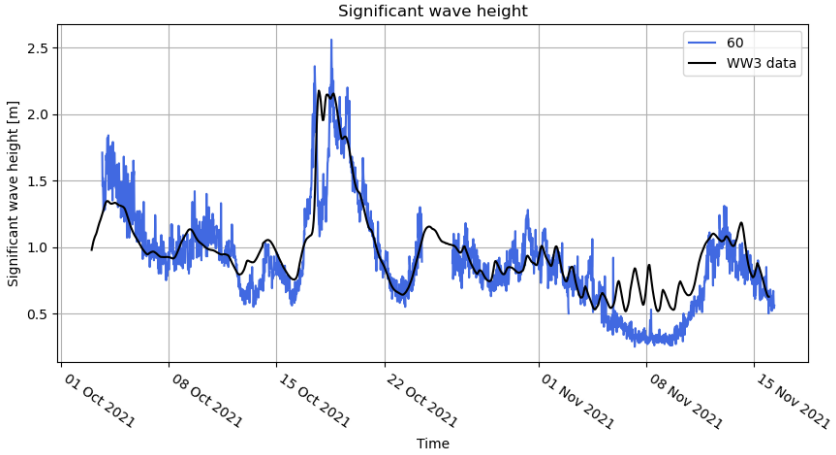

Figure K.3: Time series for the significant wave height of the WW3 point and KP60

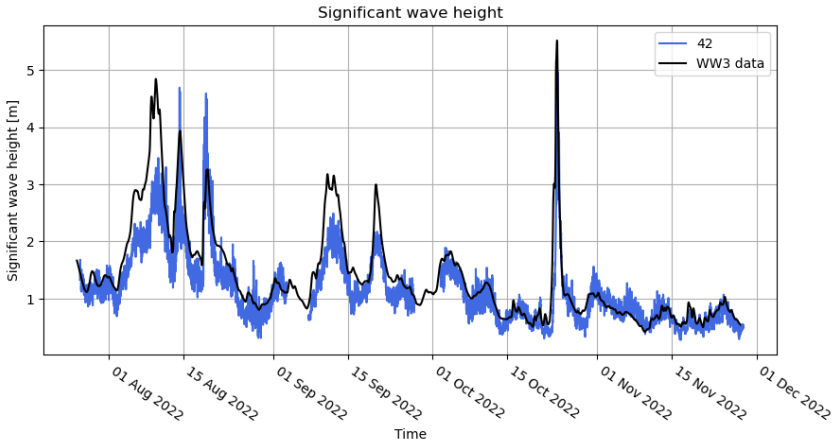

Figure K.4: Time series for the significant wave height of the WW3 point and KP42

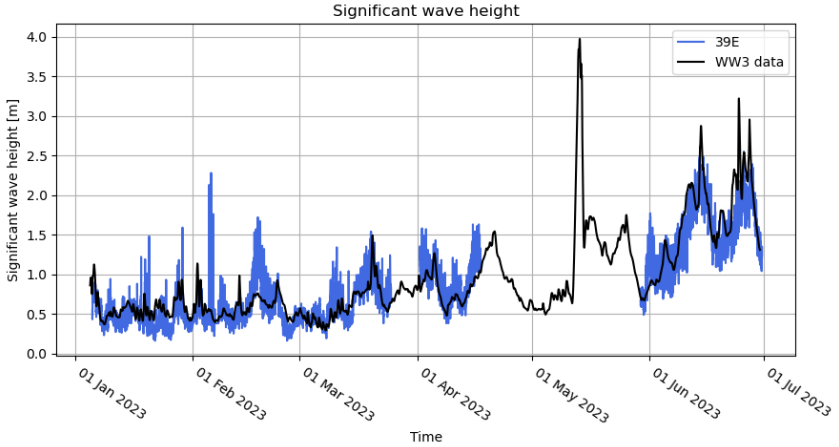

Figure K.5: Time series for the significant wave height of the WW3 point and KP39E

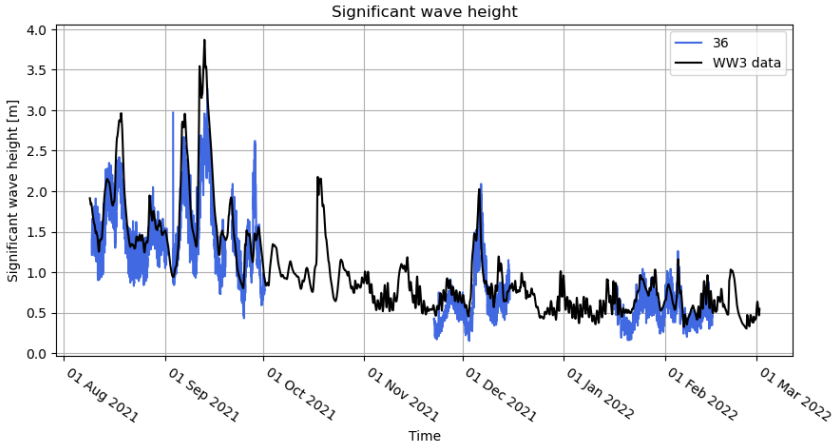

Figure K.6: Time series for the significant wave height of the WW3 point and KP36.5

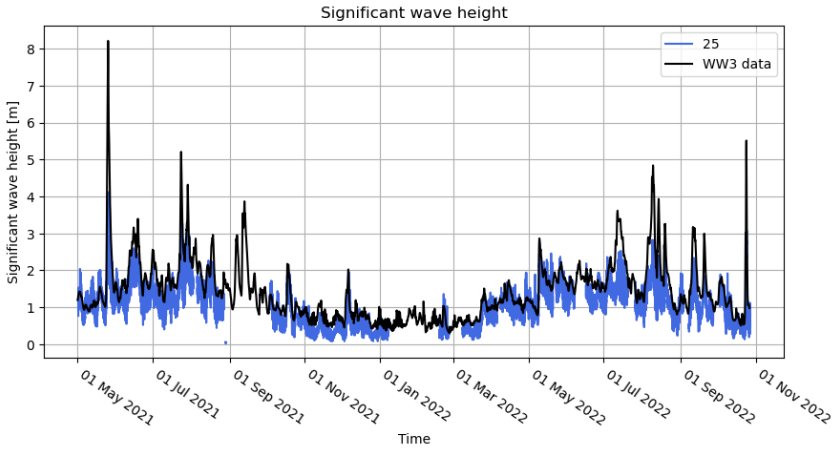

Figure K.7: Time series for the significant wave height of the WW3 point and KP25

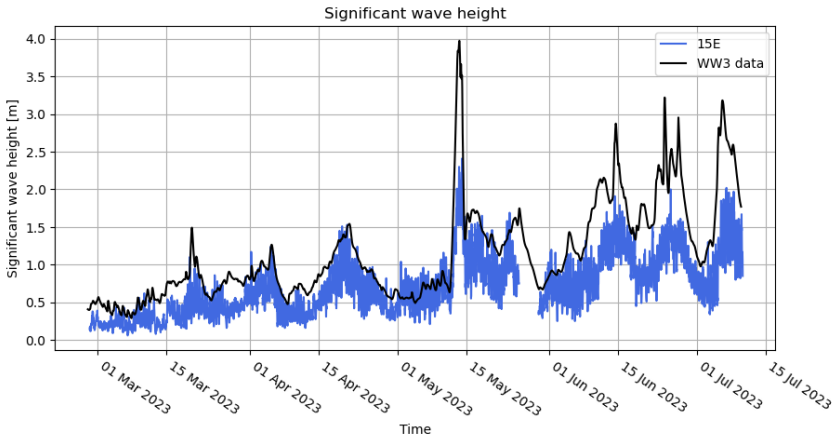

Figure K.8: Time series for the significant wave height of the WW3 point and KP15E

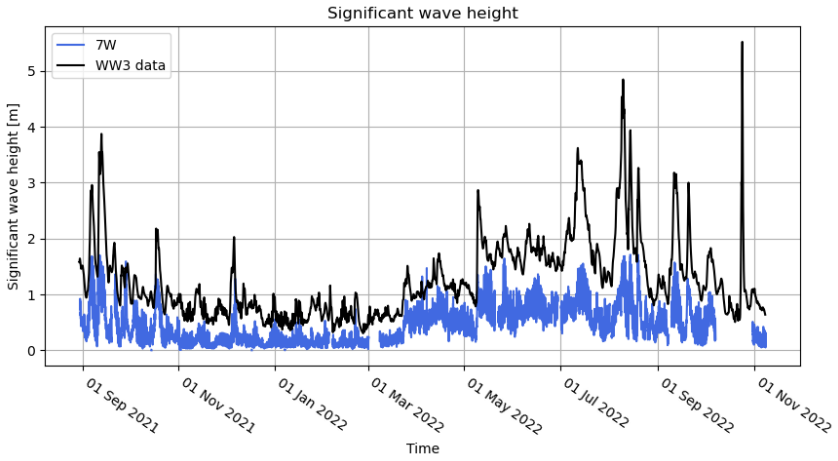

Figure K.9: Time series for the significant wave height of the WW3 point and KP7W

K.2 Comparison between buoys and SWAN model

Figures K.10 and K.11 show the significant wave heights and wave direction for 7E and 7W for the buoy measurements and SWAN data. The datasets are very similar except for the last significant wave height peak measured by buoy data and not simulated in the SWAN model. Figures K.12 and K.13 show the significant wave heights and wave direction for KP25. Again, both datasets in the figures are very similar.

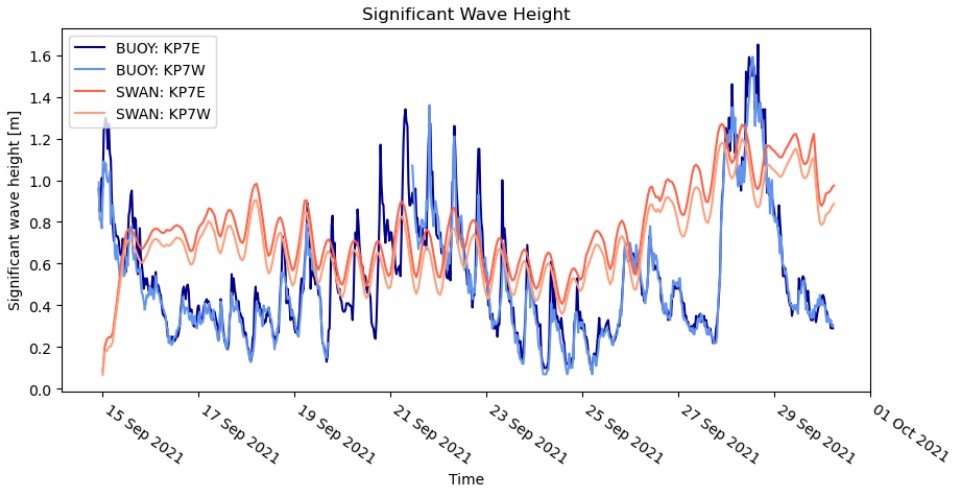

Figure K.10: Time series of the significant wave height of the buoy measurements and the SWAN model for KP7.

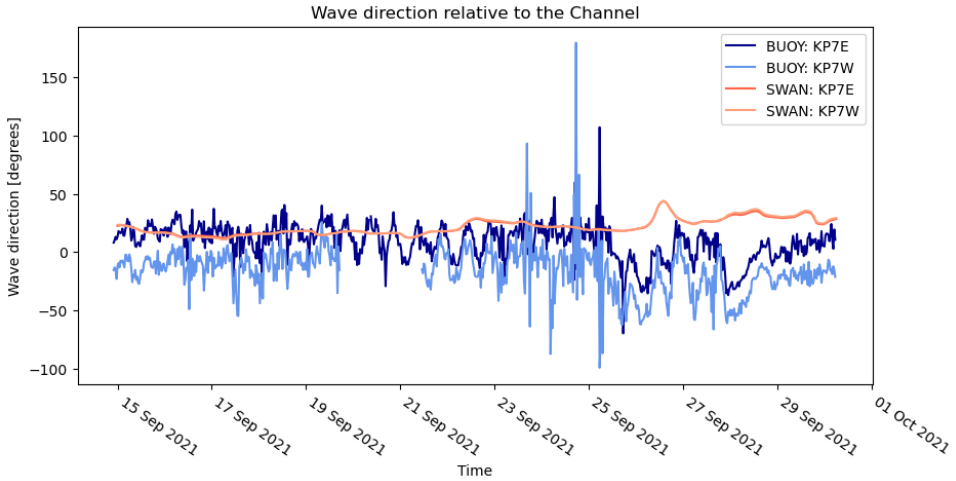

Figure K.11: Time series of the wave direction of the buoy measurements and the SWAN model for KP7.

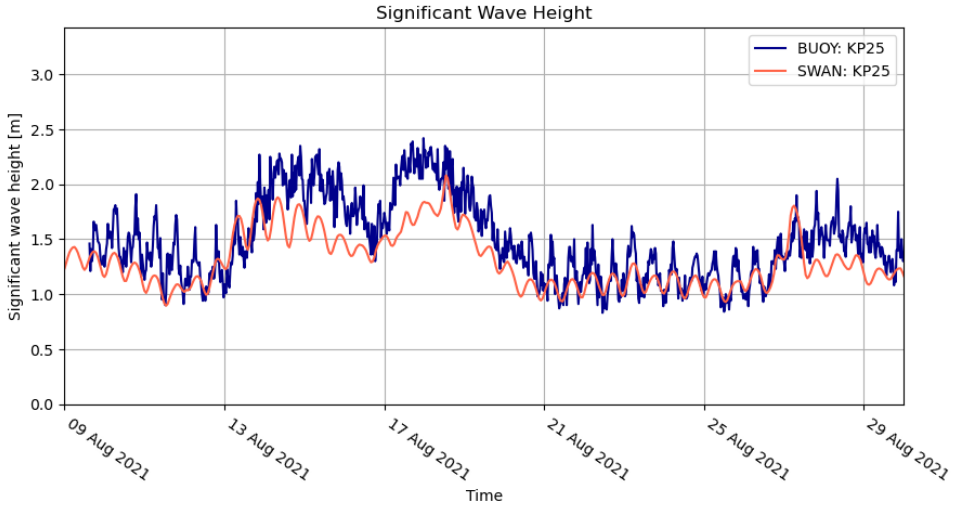

Figure K.12: Time series of the significant wave height of the buoy measurements and the SWAN model for KP25.

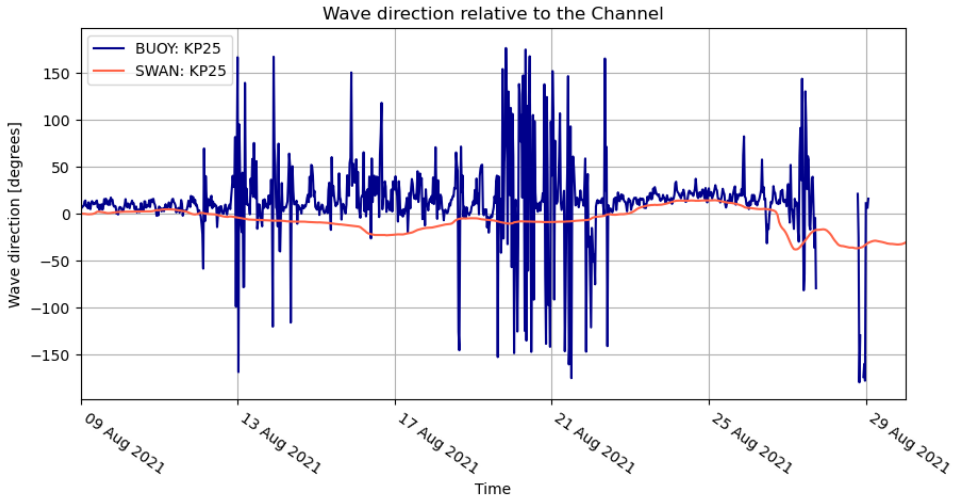

Figure K.13: Time series of the wave direction of the buoy measurements and the SWAN model for KP25.